Analysis of fine-mode aerosol retrieval capabilities by different passive remote sensing instrument designs

Kirk Knobelspiesse,[1,2,*] **Brian Cairns,**[1] **Michael Mishchenko,**[1] **Jacek Chowdhary,**[3,1] **Kostas Tsigaridis,**[3,1] **Bastiaan van Diedenhoven,**[3,1] **William Martin,**[3,1] **Matteo Ottaviani,**[1,4] **and Mikhail Alexandrov**[3,1]

[1]*NASA Goddard Institute for Space Studies, 2880 Broadway, New York, New York 10025, USA*
[2]*NASA Postdoctoral Program fellow, USA*
[3]*Columbia University, 2880 Broadway, New York, New York 10025, USA*
[4]*Stevens Institute of Technology, Hoboken, New Jersey, USA*

**kirk.knobelspiesse@nasa.gov*

Abstract: Remote sensing of aerosol optical properties is difficult, but multi-angle, multi-spectral, polarimetric instruments have the potential to retrieve sufficient information about aerosols that they can be used to improve global climate models. However, the complexity of these instruments means that it is difficult to intuitively understand the relationship between instrument design and retrieval success. We apply a Bayesian statistical technique that relates instrument characteristics to the information contained in an observation. Using realistic simulations of fine size mode dominated spherical aerosols, we investigate three instrument designs. Two of these represent instruments currently in orbit: the Multiangle Imaging SpectroRadiometer (MISR) and the POLarization and Directionality of the Earths Reflectances (POLDER). The third is the Aerosol Polarimetry Sensor (APS), which failed to reach orbit during recent launch, but represents a viable design for future instruments. The results show fundamental differences between the three, and offer suggestions for future instrument design and the optimal retrieval strategy for current instruments. Generally, our results agree with previous validation efforts of POLDER and airborne prototypes of APS, but show that the MISR aerosol optical thickness uncertainty characterization is possibly underestimated.

OCIS codes: (010.0280) Remote sensing and sensors; (010.1110) Aerosols; (010.1290) Atmospheric optics; (280.1310) Atmospheric scattering; (280.4991) Passive remote sensing.

References and links

1. IPCC. *Climate Change 2007 – The Physical Science Basis: Contribution of the Working Group I to the Fourth Assessment Report of the IPCC* (Cambridge University Press, 2007).
2. N. Loeb and W. Su, "Direct aerosol radiative forcing uncertainty based on a radiative perturbation analysis," J. Climate **23**, 5288–5293 (2010).
3. J. Hansen, M. Sato, P. Kharecha, and K. von Schuckmann, "Earth's energy imbalance and implications," Atmos. Chem. Phys. **11**, 13421–13449 (2011).
4. J. Penner, L. Xu, and M. Wang, "Satellite methods underestimate indirect climate forcing by aerosols," Proc. Natl. Acad. Sci. U.S.A. **108**, 13404–13408 (2011).

#172897 - $15.00 USD Received 19 Jul 2012; revised 24 Aug 2012; accepted 25 Aug 2012; published 4 Sep 2012

5. M. Mishchenko, B. Cairns, J. Hansen, L. Travis, R. Burg, Y. Kaufman, J. Vanderlei Martins, and E. Shettle, "Monitoring of aerosol forcing of climate from space: analysis of measurement requirements," J. Quant. Spectrosc. Radiat. Transf. **88**, 149–161 (2004).
6. Y. Kaufman, D. Tanre, and O. Boucher, "A satellite view of aerosols in the climate system," Nature **419**, 215–223 (2002).
7. M. Mishchenko, I. Geogdzhayev, B. Cairns, B. Carlson, J. Chowdhary, A. Lacis, L. Liu, W. Rossow, and L. Travis, "Past, present, and future of global aerosol climatologies derived from satellite observations: A perspective," J. Quant. Spectrosc. Radiat. Transf. **106**, 325–347 (2007).
8. M. Mishchenko, I. Geogdzhayev, L. Liu, A. Lacis, B. Cairns, and L. Travis, "Toward unified satellite climatology of aerosol properties: What do fully compatible MODIS and MISR aerosol pixels tell us?" J. Quant. Spectrosc. Radiat. Transf. **110**, 402–408 (2009).
9. R. Kahn, M. Garay, D. Nelson, K. Yau, M. Bull, B. Gaitley, J. Martonchik, and R. Levy, "Satellite-derived aerosol optical depth over dark water from MISR and MODIS: Comparisons with aeronet and implications for climatological studies," J. Geophys. Res. **112**, D18205 (2007).
10. A. Kokhanovsky, J. Deuzé, D. Diner, O. Dubovik, F. Ducos, C. Emde, M. Garay, R. Grainger, A. Heckel, M. Herman, I. Katsev, J. Keller, R. Levy, P. North, A. Prikhach, V. Rozanov, A. Sayer, Y. Ota, D. Tanré, G. Thomas, and E. Zege, "The inter-comparison of major satellite aerosol retrieval algorithms using simulated intensity and polarization characteristics of reflected light," Atmos. Meas. Tech. **3**, 909–932 (2010).
11. B. Cairns, "Polarimetric remote sensing of aerosols," Proc Geosci. Remote Sens. Symp. 518–520 (2003).
12. B. Cairns, F. Waquet, K. Knobelspiesse, J. Chowdhary, and J. Deuzé, "Polarimetric remote sensing of aerosols over land surfaces" in *Satellite Aerosol Remote Sensing over Land* (Springer, 2009), pp. 295–325.
13. M. Mishchenko, B. Cairns, G. Kopp, C. Schueler, B. Fafaul, J. Hansen, R. Hooker, T. Itchkawich, H. Maring, and L. Travis, "Accurate monitoring of terrestrial aerosols and total solar irradiance: introducing the Glory mission," Bull. Am. Meteorol. Soc. **88**, 687–691 (2007).
14. J. Chowdhary, B. Cairns, M. Mishchenko, and L. Travis, "Retrieval of aerosol properties over the ocean using multispectral and multiangle photopolarimetric measurements from the research scanning polarimeter," Geophys. Res. Lett. **28**, 243–246 (2001).
15. J. Chowdhary, B. Cairns, and L. Travis, "Case studies of aerosol retrievals over the ocean from multiangle, multispectral photopolarimetric remote sensing data," J. Atmos. Sci. **59**, 383–397 (2002).
16. J. Chowdhary, B. Cairns, M. Mishchenko, P. Hobbs, G. Cota, J. Redemann, K. Rutledge, B. Holben, and E. Russell, "Retrieval of aerosol scattering and absorption properties from photopolarimetric observations over the ocean during the clams experiment," J. Atmos. Sci. **62**, 1093–1117 (2005).
17. J. Chowdhary, B. Cairns, M. Mishchenko, and L. Travis, "Using multi-angle multispectral photo-polarimetry of the NASA Glory mission to constrain optical properties of aerosols and clouds: results from four field experiments," Proc. SPIE **5978**, 59780G (2005).
18. J. Chowdhary, B. Cairns, and L. Travis, "Contribution of water-leaving radiances to multiangle, multispectral polarimetric observations over the open ocean: bio-optical model results for case 1 waters," Appl. Opt. **45**, 5542–5567 (2006).
19. K. Knobelspiesse, B. Cairns, M. Ottaviani, R. Ferrare, J. Hair, C. Hostetler, M. Obland, R. Rogers, J. Redemann, Y. Shinozuka, A. Clarke, S. Freitag, S. Howell, V. Kapustin, and C. McNaughton, "Combined retrievals of boreal forest fire aerosol properties with a polarimeter and lidar," Atmos. Chem. Phys. **11**, 7045–7067 (2011).
20. K. Knobelspiesse, B. Cairns, J. Redemann, R. W. Bergstrom, and A. Stohl, "Simultaneous retrieval of aerosol and cloud properties during the MILAGRO field campaign," Atmos. Chem. Phys. **11**, 6245–6263 (2011).
21. F. Waquet, B. Cairns, K. Knobelspiesse, J. Chowdhary, L. Travis, B. Schmid, and M. Mishchenko, "Polarimetric remote sensing of aerosols over land," J. Geophys. Res. **114**, D01206 (2009).
22. V. Zubko, Y. Kaufman, R. Burg, and J. Martins, "Principal component analysis of remote sensing of aerosols over oceans," IEEE Trans. Geosci. Remote Sens. **45**, 730–745 (2007).
23. D. Tanre, M. Herman, and Y. Kaufman, "Information on aerosol size distribution contained in solar reflected spectral radiances," J. Geophys. Res. **101**, 19,043–19,060 (1996).
24. O. Kalashnikova, M. Garay, A. Davis, D. Diner, and J. Martonchik, "Sensitivity of multi-angle photo-polarimetry to vertical layering and mixing of absorbing aerosols: Quantifying measurement uncertainties," J. Quant. Spectrosc. Radiat. Transf. **112**, 2149–2163 (2011).
25. C. Rodgers, *Inverse Methods for Atmospheric Sounding: Theory and Practice* (World Scientific, 2000).
26. O. Hasekamp and J. Landgraf, "Retrieval of aerosol properties over land surfaces: capabilities of multiple-viewing-angle intensity and polarization measurements," Appl. Opt. **46**, 3332–3344 (2007).
27. O. P. Hasekamp, "Capability of multi-viewing-angle photo-polarimetric measurements for the simultaneous retrieval of aerosol and cloud properties," Atmos. Meas. Tech. **3**, 839–851 (2010).
28. C. Rodgers and B. Connor, "Intercomparison of remote sounding instruments," J. Geophys. Res. **108**, D34116 (2008).
29. J. Hansen and L. Travis, "Light scattering in planetary atmospheres," Space Sci. Rev. **16**, 527–610 (1974).
30. J. de Haan, P. Bosma, and J. Hovenier, "The adding method for multiple scattering calculations of polarized light," Astron. Astrophys. **183**, 371–391 (1987).

#172897 - $15.00 USD Received 19 Jul 2012; revised 24 Aug 2012; accepted 25 Aug 2012; published 4 Sep 2012

31. W. De Rooij and C. Van der Stap, "Expansion of Mie scattering matrices in generalized spherical functions," Astron. Astrophys. **131**, 237–248 (1984).
32. J. Chowdhary, B. Cairns, F. Waquet, K. Knobelspiesse, M. Ottaviani, J. Redemann, L. Travis, and M. Mishchenko, "Sensitivity of multiangle, multispectral polarimetric remote sensing over open oceans to water-leaving radiance: Analyses of RSP data acquired during the MILAGRO campaign," Remote Sens. Environ. **118**, 284–308 (2012).
33. C. Cox and W. Munk, "Measurement of the roughness of the sea surface from photographs of the sun's glitter," J. Opt. Soc. Am. **44**, 838–850 (1954).
34. F. Nicodemus, *Geometrical Considerations and Nomenclature for Reflectance* (US Dept. of Commerce, National Bureau of Standards, US Govt. Print. Off., 1977).
35. G. Schaepman-Strub, M. Schaepman, T. Painter, S. Dangel, and J. Martonchik, "Reflectance quantities in optical remote sensing: definitions and case studies," Remote Sens. Environ. **103**, 27–42 (2006).
36. W. Lucht, C. Schaaf, and A. Strahler, "An algorithm for the retrieval of albedo from space using semiempirical BRDF models," IEEE Trans. Geosci. Remote Sens. **38**, 977–998 (2000).
37. C. Schaaf, F. Gao, A. Strahler, W. Lucht, X. Li, T. Tsang, N. Strugnell, X. Zhang, Y. Jin, and J. Muller, "First operational BRDF, albedo nadir reflectance products from MODIS," Remote Sens. Environ. **83**, 135–148 (2002).
38. C. Schaaf, A. Strahler, M. Roman, J. Salomon, and J. Hodges. "Assessment of albedo derived from the moderate-resolution imaging spectroradiometer at the Southern Great Plains site," in *Proceedings of the Sixteenth ARM Science Team Meeting* (Alburquerque, NM, 2006).
39. K. Knobelspiesse, B. Cairns, C. Schaaf, B. Schmid, and M. Román, "Surface BRDF estimation from an aircraft compared to MODIS and ground estimates at the Southern Great Plains site," J. Geophys. Res. **113**, D20105 (2008).
40. L. Curier, G. de Leeuw, P. Kolmonen, A.-M. Sundstrom, L. Sogacheva, and Y. Bennouna, "Aerosol retrieval over land using the (A)ATSR dual-view algorithm," in *Satellite Aerosol Remote Sensing over Land* (Springer, 2009).
41. W. Grey and P. North. "Aerosol optical depth from dual-view (A)ATSR satellite observations," in *Satellite Aerosol Remote Sensing over Land* (Springer, 2009).
42. F. Breon, D. Tanré, P. Lecomte, and M. Herman, "Polarized reflectance of bare soils and vegetation: measurements and models," IEEE Trans. Geosci. Remote Sens. **33**, 487–499 (1995).
43. F. Nadal and F.-M. Breon, "Parameterization of surface polarized reflectance derived from POLDER spaceborne measurements," IEEE Trans. Geosci. Remote Sens. **37**, 1709 (1999).
44. P. Litvinov, O. Hasekamp, B. Cairns, and M. Mishchenko, "Reflection models for soil and vegetation surfaces from multiple-viewing angle photopolarimetric measurements," J. Quant. Spectrosc. Radiat. Transfer **111**, 529–539 (2010).
45. B. Holben, Y. Kaufman, T. Eck, I. Slutsker, D. Tanre, J. Buis, A. Setzer, E. Vermote, and J. Reagan, "AERONET – a federated instrument network and data archive for aerosol characterization," Remote Sens. Environ. **66**, 1–16 (1998).
46. O. Dubovik, B. Holben, T. Eck, A. Smirnov, Y. Kaufman, M. King, D. Tanré, and I. Slutsker, "Variability of absorption and optical properties of key aerosol types observed in worldwide locations," J. Atmos. Sci. **59**, 590–608 (2002).
47. G. Myhre, T. Berglen, M. Johnsrud, C. Hoyle, T. Berntsen, S. Christopher, D. Fahey, I. Isaksen, T. Jones, R. Kahn, N. Loeb, P. Quinn, L. Remer, S. Schwartz, K. Yttri, "Modelled radiative forcing of the direct aerosol effect with multi-observation evaluation," Atmos. Chem. Phys. **9**, 1365–1392 (2009).
48. M. Ottaviani, B. Cairns, J. Chowdhary, B. Van Diedenhoven, K. Knobelspiesse, C. Hostetler, R. Ferrare, S. Burton, J. Hair, M. Obland, and R. Rogers, "Polarimetric retrievals of surface and cirrus clouds properties in the region affected by the deepwater horizon oil spill," Remote Sens. Environ. **121**, 389–403 (2012).
49. Y. Kawata, "Circular polarization of sunlight reflected by planetary atmospheres," Icarus **33**, 217–232 (1978).
50. M. Mishchenko, L. Travis, and A. Lacis, *Multiple Scattering of Light by Particles: Radiative Transfer and Coherent Backscattering* (Cambridge Univ. Press, 2006).
51. S. Persh, Y. Shaham, O. Benami, B. Cairns, M. Mishchenko, J. Hein, and B. Fafaul, "Ground performance measurements of the Glory aerosol polarimetry sensor," Proc. SPIE **7807**, 780703 (2010).
52. Y. Kaufman, D. Tanré, L. Remer, E. Vermote, A. Chu, and B. Holben, "Operational remote sensing of tropospheric aerosol over land from EOS moderate resolution imaging spectroradiometer," J. Geophys. Res. **102**, 17,051–17,067 (1997).
53. M. King, W. Menzel, Y. Kaufman, D. Tanré, B. Gao, S. Platnick, S. Ackerman, L. Remer, R. Pincus, and P. Hubanks, "Cloud and aerosol properties, precipitable water, and profiles of temperature and water vapor from MODIS," IEEE Trans. Geosci. Remote Sens. **41**, 442–458 (2003).
54. L. A. Remer, R. G. Kleidman, R. C. Levy, Y. Kaufman, D. Tanré, S. Mattoo, J. V. Martins, C. Ichoku, I. Koren, H. Yu, and B. Holben, "Global aerosol climatology from the MODIS satellite sensors," J. Geophys. Res. **113**, D14S07 (2008).
55. R. Levy, L. Remer, R. Kleidman, S. Mattoo, C. Ichoku, R. Kahn, and T. Eck, "Global evaluation of the collection 5 MODIS dark-target aerosol products over land," Atmos. Chem. Phys. **10**, 10399–10420 (2010).
56. D. Diner, J. Beckert, T. Reilly, C. Bruegge, J. Conel, R. Kahn, J. Martonchik, T. Ackerman, R. Davies, S. Gerstl,

#172897 - $15.00 USD Received 19 Jul 2012; revised 24 Aug 2012; accepted 25 Aug 2012; published 4 Sep 2012

H. Gordon, J. Muller, R. Myneni, P. Sellers, B. Pinty, and M. Verstraete, "Multi-angle Imaging SpectroRadiometer (MISR) instrument description and experiment overview," IEEE Trans. Geosci. Remote Sens. **36**, 1072–1087 (1998).
57. J. Martonchik, D. Diner, K. Crean, and M. Bull, "Regional aerosol retrieval results from MISR," IEEE Trans. Geosci. Remote Sens. **40**, 1520–1532 (2002).
58. J. Martonchik, R. Kahn, and D. Diner. "Retrieval of aerosol properties over land using MISR observations," in *Satellite Aerosol Remote Sensing over Land* (Springer, 2009), pp. 267–293.
59. C. Bruegge, W. Abdou, D. Diner, B. Gaitley, M. Helmlinger, R. Kahn, and J. Martonchik. "Validating the MISR radiometric scale for the ocean aerosol science communities." in *Proceedings of The International Workshop on Radiometric and Geometric Calibration* (AA. Balkema Publishers, 2004).
60. D. Tanré, F. M. Bréon, J. L. Deuzé, O. Dubovik, F. Ducos, P. François, P. Goloub, M. Herman, A. Lifermann, and F. Waquet, "Remote sensing of aerosols by using polarized, directional and spectral measurements within the A-train: the PARASOL mission," Atmos. Meas. Tech. **4**, 1383–1395 (2011).
61. T. Anderson, R. Charlson, N. Bellouin, O. Boucher, M. Chin, S. Christopher, J. Haywood, Y. Kaufman, S. Kinne, J. Ogren, L. A. Remer, T. Takemure, D. Tanré, O. Torres, C. Trepte, B. Wielicki, D. Winker, and H. Yu, "An "A-Train" strategy for quantifying direct climate forcing by anthropogenic aerosols," Bull. Am. Meteorol. Soc. **86**, 1795–1809 (2005).
62. P. Deschamps, F. Bréon, M. Leroy, A. Podaire, A. Bricaud, J. Buriez, and G. Seze, "The POLDER mission: Instrument characteristics and scientific objectives," IEEE Trans. Geosci. Remote Sens. **32**, 598–615 (1994).
63. O. Dubovik, M. Herman, A. Holdak, T. Lapyonok, D. Tanré, J. L. Deuzé, F. Ducos, A. Sinyuk, and A. Lopatin, "Statistically optimized inversion algorithm for enhanced retrieval of aerosol properties from spectral multi-angle polarimetric satellite observations," Atmos. Meas. Tech. **4**, 975–1018 (2011).
64. O. Hasekamp, P. Litvinov, and A. Butz, "Aerosol properties over the ocean from parasol multiangle photopolarimetric measurements," J. Geophys. Res. **116**, D14204 (2011).
65. B. Fougnie, G. Bracco, B. Lafrance, C. Ruffel, O. Hagolle, and C. Tinel, "PARASOL in-flight calibration and performance," Appl. Opt. **46**, 5435–5451 (2007).
66. D. Diner, W. Abdou, C. Bruegge, J. Conel, K. Crean, B. Gaitley, M. Helmlinger, R. Kahn, J. Martonchik, S. Pilorz, and B. Holben," "MISR aerosol optical depth retrievals over southern Africa during the SAFARI-2000 dry season campaign," Geophys. Res. Lett. **28**, 3127–3130 (2001).
67. S. Christopher and J. Wang, "Intercomparison between multi-angle imaging spectroradiometer (MISR) and sunphotometer aerosol optical thickness in dust source regions over China: implications for satellite aerosol retrievals and radiative forcing calculations," Tellus, Ser. B **56**, 451–456 (2004).
68. Y. Liu, J. Sarnat, B. Coull, P. Koutrakis, and D. Jacob, "Validation of multiangle imaging spectroradiometer (MISR) aerosol optical thickness measurements using aerosol robotic network (AERONET) observations over the contiguous United States," J. Geophys. Res. **109**, D06205 (2004).
69. J. Martonchik, D. Diner, R. Kahn, B. Gaitley, and B. Holben, "Comparison of MISR and AERONET aerosol optical depths over desert sites," Geophys. Res. Lett. **31**, L16102 (2004).
70. R. Kahn, B. Gaitley, J. Martonchik, D. Diner, K. Crean, and B. Holben. "Multiangle Imaging Spectroradiometer (MISR) global aerosol optical depth validation based on 2 years of coincident Aerosol Robotic Network (AERONET) observations," J. Geophys. Res. **110**, D10S04 (2005).
71. W. Abdou, D. Diner, J. Martonchik, C. Bruegge, R. Kahn, B. Gaitley, K. Crean, L. Remer, and B. Holben, "Comparison of coincident multiangle imaging spectroradiometer and moderate resolution imaging spectroradiometer aerosol optical depths over land and ocean scenes containing aerosol robotic network sites," J. Geophys. Res. **110**, D10S07 (2005).
72. X. Jiang, Y. Liu, B. Yu, and M. Jiang, "Comparison of MISR aerosol optical thickness with AERONET measurements in Beijing metropolitan area," Remote Sens. Environ. **107**, 45–53 (2007).
73. M. Mishchenko, L. Liu, L. Travis, B. Cairns, and A. Lacis, "Toward unified satellite climatology of aerosol properties: 3. MODIS versus MISR versus AERONET," J. Quant. Spectrosc. Radiat. Transf. **111**, 540–552 2010.
74. R. Levy, L. Remer, D. Tanré, Y. Kaufman, C. Ichoku, B. Holben, J. Livingston, P. Russell, and H. Maring, "Evaluation of the moderate-resolution imaging spectroradiometer (MODIS) retrievals of dust aerosol over the ocean during PRIDE," J. Geophys. Res. **108**, D198594 (2003).
75. L. Remer, Y. Kaufman, D. Tanré, S. Mattoo, D. Chu, J. Martins, R. Li, C. Ichoku, R. Levy, R. Kleidman, T. Eck, E. Vermote, and B. Holben, "The MODIS aerosol algorithm, products, and validation," J. Atmos. Sci. **62**, 947–973 (2005).
76. L. Remer, Y. Kaufman, and R. Kleidman, "Comparison of three years of Terra and Aqua MODIS aerosol optical thickness over the global oceans," IEEE Lett. Geosci. Remote Sens. **3**, 537– 540 (2006).
77. R. Kahn, D. Nelson, M. Garay, R. Levy, M. Bull, D. Diner, J. Martonchik, S. Paradise, E. Hansen, and L. Remer, "MISR aerosol product attributes and statistical comparisons with MODIS," IEEE Trans. Geosci. Remote Sens. **47**, 4095–4114 (2009).

#172897 - $15.00 USD Received 19 Jul 2012; revised 24 Aug 2012; accepted 25 Aug 2012; published 4 Sep 2012

1. Introduction

Aerosols, which are suspended particulate matter in the atmosphere, are widely considered to be one of the most uncertain components of the global climate with important influence on cloud properties and radiative forcing. The global radiative forcing due to aerosols is potentially as large as that of greenhouse gases (but with the opposite sign). However, climate models, which express our current understanding and are required to predict future change, produce a wide variety of aerosol forcing values. Indeed, the Intergovernmental Panel on Climate Change (IPCC), in its Fourth Assessment Report, describes the scientific understanding of the aerosol direct radiative effect as "medium-low", while the understanding of indirect effects (primarily associated with modifying clouds) considered to be "low" [1]. More recent research has shown that even this assessment is probably optimistic and that aerosol forcing could be larger than previously expected (for example [2–4]).

Accurate climate modeling necessitates an understanding of aerosol sources, transport, sinks, optical properties and climate interactions. This, in turn, requires observations of aerosols from orbit, since a long term, statistical understanding of aerosols throughout the globe is needed [3, 5]. For several decades, the field of aerosol remote sensing has undergone rapid technological development. Yet, even with the capabilities of today's state-of-the-art orbital instruments [6], significant biases between global measurements by different instruments of aerosol optical properties remain [7–10]. Furthermore, most instruments do not provide information about all the parameters needed to reduce uncertainties in the radiative forcing due to aerosols [5]. These parameters include aerosol total atmospheric extinction, size distribution, particle shape, complex refractive index and vertical distribution, generally for multiple size modes. For passive instruments (those that detect reflected solar radiation), shortcomings are generally due to the limited information available in the measurements. Essentially, the process by which aerosol parameters are determined from observations is often underdetermined. As a result, accurate and independent values of only some parameters can be extracted from the data, while others must be assumed based upon external information or historical observations. The impact of these assumptions on retrieval uncertainty is often difficult to characterize [9, 10].

For these reasons, an alternative, but complementary, aerosol remote sensing approach is to maximize the information observed in each scene, even if it is at the expense of spatial and temporal resolution. This was the underlying design principle for the Aerosol Polarimetry Sensor (APS), an instrument on the NASA Glory mission, and its airborne prototype, the Research Scanning Polarimeter (RSP) [11–13]. Unfortunately, Glory failed to reach orbit when it was launched in March, 2011, but the decade of observations from aircraft by the RSP [14–21] demonstrate the validity of this design and its potential for use in future orbital missions. Both RSP and APS designs make multi-angle, multi-spectral observations of total and linearly polarized reflectance. While there are minor differences between the two, both RSP and APS have nine spectral channels between 410 and 2260nm, a high degree of polarimetric accuracy ($\leq$0.2%) and many view angles (about 150 for RSP, more than 250 for APS, over a viewing angle range of $\pm 60^{\circ}$ from nadir). In order to obtain the large viewing angle range and high density of angular sampling, both instruments are scanners, not imagers, which means the swath width is a single pixel wide [13]. While this limits the ability of an instrument such as this to track individual aerosol related processes, it allows for the simultaneous retrieval of nearly all the relevant aerosol optical properties in a scene, which is required to determine aerosol radiative forcing on relevant spatial and temporal scales. The advantage of this approach is that more parameters can be retrieved, and they are much less dependent upon the selection of *a priori* aerosol properties. Furthermore, retrieval uncertainties can be accurately assessed [12, 19–21].

As instruments become more complex, it becomes increasingly difficult to intuitively link the aerosol parameter retrieval capability to particular measurement characteristics (especially

#172897 - $15.00 USD Received 19 Jul 2012; revised 24 Aug 2012; accepted 25 Aug 2012; published 4 Sep 2012

when using polarimetric observations). For this reason, sensitivity studies are an important aspect of instrument design and assessment, and are particularly germane in the aftermath of the Glory launch failure to determine sensor requirements for future missions. A study such as this is particularly timely for this reason. There are a variety of types of sensitivity studies, all involving the simulation of observations using a radiative transfer computational technique. For example, Zubko et al. [22] and Tanré et al. [23] performed a principal components analysis of many simulated scenes to determine the number of parameters that can be extracted from a particular measurement configuration. While this is a straightforward way of assessing the information contained in a measurement, it is difficult to directly include observational uncertainty as a part of this technique, especially if an observation contains measurements with a variety of uncertainties (as is the case when combining total and polarized reflectance with instruments such as the APS). Another approach is the so-called "z-score" method, where the difference between a pair of simulations is compared to observational uncertainty. This is often used to investigate the sensitivity to specific conditions. Kalashnikova et al. [24] used this technique to analyze the sensitivity of multiangle, polarimetric observations to the vertical distribution of absorbing aerosols.

The most widely accepted sensitivity study method uses radiative transfer simulations to project observational error into the parameter domain using the sensitivity of the radiative transfer simulation to parameter perturbations. This approach, which provides estimates of aerosol parameter retrieval uncertainty, is described formally in the book by Rodgers [25], and has been used for aerosol and cloud passive remote sensing studies by Knobelspiesse et al., Hasekamp and Landgraf and Hasekamp [20, 26, 27]. We use this method, since results are expressed in terms of retrieval uncertainty, and because measurement uncertainty and configuration can be explicitly specified. Of course, all sensitivity studies represent a simplification of the scenario that would be encountered in a retrieval using real data. In this work, we attempt to make the study as realistic as possible, by simulating a large number of aerosol and surface optical properties whose values are drawn from the best available observational data. Results in this paper should be seen as the best possible retrieval uncertainty. In addition to estimating retrieval uncertainty, we also compute the Shannon Information Content (SIC), which indicates the total quantity of information that a measurement adds to our knowledge of the retrieved parameters. Although studies such as this represent simplified versions of the real world, they are highly valuable in order to establish the minimum instrument configuration and accuracy requirements needed to meet retrieval demands.

This is not the first study to use these techniques to assess aerosol retrieval uncertainty. However, it is unique in that special efforts have been made to ensure the suitability of the aerosol models, and an investigation of retrieval uncertainty sensitivity to model characteristics is performed. We then provide a direct comparison of three major instrument designs, and investigate the implications that this comparison has on previous estimates of uncertainty. These designs include the Multiangle Imaging SpectroRadiometer (MISR) on the NASA Terra spacecraft, the POLarization and Directionality of the Earths Reflectances (POLDER) instrument on the CNES PARASOL (Polarization and Anisotropy of Reectances for Atmospheric Sciences coupled with Observations from a Lidar) spacecraft, and the APS/RSP instrument design described above. Finally, we show how this technique can be used to choose the optimal measurement strategy using an example that tests the utility of total reflectance observations for retrieval of aerosol properties over land.

Section 2 of this paper is a description of the details of the sensitivity study method and the specifics of its implementation, while section 3 shows results for a variety of scenarios analogous to existing and planned sensor designs. Results are discussed in section 4 in the context of the observational needs of the community, and a brief conclusion is in section 5.

#172897 - $15.00 USD Received 19 Jul 2012; revised 24 Aug 2012; accepted 25 Aug 2012; published 4 Sep 2012

2. Methodology

2.1. Error propagation

The sensitivity study presented in this work is based upon the Bayesian approach using Gaussian distributions as described in [25]. This method estimates retrieval uncertainty given an observational configuration and uncertainty with the Eq.

$$\hat{\mathbf{S}}^{-1} = \mathbf{K}^T \mathbf{S}_\varepsilon^{-1} \mathbf{K} + \mathbf{S}_a^{-1}, \tag{1}$$

where $\hat{\mathbf{S}}$ is the retrieval error covariance matrix, $\mathbf{S}_\varepsilon$ is the observation error covariance matrix, $\mathbf{S}_a$ is the *a priori* error covariance matrix, $\mathbf{K}$ is the Jacobian (forward model sensitivity) matrix, ^{T} denotes the transpose, and $^{-1}$ denotes the inverse. The observation error covariance matrix represents measurement uncertainty, where the square roots of the standard errors associated with each individual measurement (corresponding to a single view angle, wavelength, and polarization state) are on the diagonal, while off-diagonal elements represent the strength of error correlations. $\mathbf{S}_\varepsilon$ is square with the dimension of the number of measurements, $[m \times m]$, made with each observation. The retrieval error covariance matrix, $\hat{\mathbf{S}}$, has a similar structure, but represents the uncertainty in parameters retrieved from the data and has the dimension of the number of retrieved parameters, $[n \times n]$. Essentially, it is the projection of observational uncertainties into state (parameter) space. The Jacobian matrix, $\mathbf{K}$, expresses the sensitivity of the model to changes in the parameters to be retrieved. Radiative transfer simulations, indicated by the function $\mathbf{F}(\mathbf{x})$ (where $\mathbf{x}$ is a vector atmospheric and surface optical parameters), can be used to estimate the Jacobian matrix

$$K_{ij}(\mathbf{x}) = \frac{\partial F_i(\mathbf{x})}{\partial x_j} \approx \frac{F_i(\mathbf{x}') - F_i(\mathbf{x})}{x'_j - x_j}, \tag{2}$$

where the partial derivative of the radiative transfer model, $\mathbf{F}(\mathbf{x})$, for the simulated set of parameters, $\mathbf{x}$, is computed for each observation, i, and each parameter, j. This matrix therefore has the dimension of $[m \times n]$. In this study, Eq. (2) is estimated numerically, by perturbing the jth element of $\mathbf{x}$ (as indicated by $\mathbf{x}'$) and recalculating the forward model. We use a small perturbation (0.05%, or larger if machine precision becomes relevant) so that we can assume $\mathbf{F}(\mathbf{x})$ is linear over the perturbation. While this true in the vicinity of a given aerosol state, $\mathbf{F}(\mathbf{x})$ is most likely nonlinear over the entire domain, so the Jacobian must be reassessed for each possible combination of parameters representing a scene. For this reason, we compute a variety of Jacobians representing various plausible atmospheric conditions, and evaluate the averaged retrieval uncertainty in $\hat{\mathbf{S}}$. The selection of the conditions used to compute the set of Jacobians is described in more detail in section 2.4.

The final component of Eq. (1) is the *a priori* error covariance matrix, $\mathbf{S}_a$. This matrix represents the quantity of information known about a scene prior to measurement. For example, we know that the Aerosol Optical Thickness (AOT) must be greater than zero and is probably less than one, that the real refractive index is greater than or equal to that of water (around 1.33, depending on wavelength), and so forth. $\mathbf{S}_a$ thus represents the uncertainty prior to measurement (on the diagonal) and the correlation between parameters off the diagonal. Like for the observational error covariance matrix, we assume that there are no correlations between parameters in the *a priori* covariance matrix. Since it describes parameter specific quantities, the *a priori* error covariance matrix has the dimension of $[n \times n]$.

Eq. (1) provides a straightforward way of linking the characteristics of a set of observations to the retrieval uncertainty. The square roots of the diagonals of $\hat{\mathbf{S}}$ are the one-sigma uncertainties given the observation uncertainties, forward model sensitivity to retrieved parameters, and prior knowledge of the scene. Off diagonal elements represent the correlation between pairs

#172897 - $15.00 USD Received 19 Jul 2012; revised 24 Aug 2012; accepted 25 Aug 2012; published 4 Sep 2012

of retrieved parameters. Real world retrievals will most likely have larger uncertainties and biases, as this method assumes that the forward model is a perfect representation of the scene, observations are well described by the covariance matrix $\mathbf{S}_\varepsilon$ and that a retrieval algorithm can successfully converge to a solution. Of these concerns, forward model error and convergence are the most significant. For example, surface reflectance may not be adequately described by the limited set of parameters used for that purpose. Regarding convergence, requirements in processing speed for global datasets may require algorithms that are not fully capable of extracting information of the lowest possible uncertainty.

This method provides an estimate for the retrieval uncertainty in the vicinity of the actual solution, and applying it over a wide range of aerosol loads and microphysical models allows the potential capabilities of a measurement system to be evaluated. What makes this technique powerful is that it can be used to test a variety of instrument configurations with little computational effort. For example, we can directly see the impact of changing polarimetric accuracy on the retrieval of aerosol refractive index, or the influence that certain channels have on the ability to determine the aerosol size distribution. If the Jacobians are computed for a wide variety of types of scenes, the forward model computations do not need to be recalculated: $\hat{\mathbf{S}}$ can be recalculated for various $\mathbf{S}_\varepsilon$ and $\mathbf{S}_a$ using the subset of $\mathbf{K}$ that is appropriate for the specific measurement configuration. The only computational expense involves matrix multiplication and computation of the inverse of $\hat{\mathbf{S}}$, $\mathbf{S}_\varepsilon$ and $\mathbf{S}_a$. Computing $\hat{\mathbf{S}}^{-1}$ and $\mathbf{S}_a^{-1}$ is usually trivial, since n, the number of parameters and dimension of these covariance matrices, is generally less than twenty. If the number of observations, m is large (it is in the hundreds or thousands for multi-angle, multi-spectral instruments), then the $\mathbf{S}_\varepsilon^{-1}$ computation can become expensive.

$\hat{\mathbf{S}}$ can also be used to determine the estimated uncertainty for parameters that are not directly retrieved, as long as those parameters can be uniquely expressed by the parameters in $\mathbf{x}$ [26]. If a parameter is defined by some function, say $a = G(\mathbf{x})$, then the uncertainty of a will be

$$\sigma_a = \sqrt{\sum_{i=1}^{n}\sum_{j=1}^{n} \hat{\mathbf{S}}_{i,j} \frac{\partial a}{\partial x_i}\frac{\partial a}{\partial x_j}}. \tag{3}$$

In this study, we use Eq. (3) to compute the uncertainty in the Single Scattering Albedo (SSA) and the total AOT for all aerosol size modes.

2.2. Information content

While Eq. (1) is a very powerful tool that links the observational configuration to the retrieval uncertainty, it is useful to have a scalar parameter representing the the total information contained in a measurement. We use the Shannon Information Content (SIC), which we will denote by H [25]. The SIC was originally intended to describe communication capacity and as a tool for the optimal compression of messages. Mathematically, it has similarites to the concept of entropy in thermodynamics. H represents the reduction of "entropy" in state space due to an observation, where entropy is taken to mean the volume of possible solutions in state space that are consistent with our understanding of the scene. The act of making a measurement excludes some portion of state space that can no longer represent the scene, and H is a measure of the volume of this excluded portion. We compute the SIC using the formula

$$H = \frac{1}{2}\ln|\hat{\mathbf{S}}^{-1}\mathbf{S}_a|, \tag{4}$$

where $|\cdot|$ indicates the determinant of the enclosed matrix. This formulation is appropriate for Gaussian probability distributions, and is thus applicable for each $\hat{\mathbf{S}}$ corresponding to a particular aerosol simulation (expressed as $\mathbf{K}$ in Eq. (1)). H is proportional to the natural logarithm of the ratio of the *a priori* volume (expressed as the determinant) to the volume after

#172897 - $15.00 USD Received 19 Jul 2012; revised 24 Aug 2012; accepted 25 Aug 2012; published 4 Sep 2012

a measurement. H is therefore larger for measurements containing greater information. The SIC is dependent upon the dimensionality of $\hat{\mathbf{S}}$ and $\mathbf{S}$, so we use the subset of space representing aerosol parameters only. This provides for a more impartial comparison of measurements, although the correlations between aerosol and other parameters are ignored [28]. This is also the reason we choose to compute the SIC in state space, although it can also be computed in measurement space, as is described in section 2.5 of [25].

2.3. The forward model and Jacobian matrix

The Jacobian matrix, $\mathbf{K}$, represents the sensitivity of the forward model, $\mathbf{F}(\mathbf{x})$, to perturbations in the model parameters, $\mathbf{x}$. $\mathbf{F}(\mathbf{x})$ is a simulation of a plausible scene of aerosols suspended over an ocean or land surface, with parameters describing the aerosol optical properties and surface reflectance contained in the vector $\mathbf{x}$. Our simulations use nested models, where aerosol single scattering properties are computed for bi-modal, log-normal size distributions of spherical aerosols using the Lorenz-Mie solution of Maxwell's equations as described in Hansen and Travis, [29]. The doubling/adding calculations have been verified to be within 1% (average absolute devation 0.03%) in radiance and 0.08% (average absolute deviation 0.02%) in *DoLP* of the results given in de Haan, Bosma and Hovenier [30]. Those results use the output from a Mie code for a Haze L distribution documented in de Rooij and van der Stap [31]. The overall performance of the code (including the Mie code) used here is therefore considered to be valid against benchmark literature results at the 1% worst case, 0.03% average in radiance, and 0.1% worst case and 0.02% average in *DoLP* (see section 2.5 for a description of the *DoLP* polarimetric quantity).

For each size mode, the aerosol size distribution is specified using an effective radius, r_e, and variance, v_e, as defined in [29]. Globally, bimodal aerosol size distributions are a common occurrence. "Fine" size mode aerosols generally have an effective radius between 0.1 and 0.25 μm and are the result of chemical processes such as combustion and photo-oxidation, while "Coarse" mode aerosols are mechanically generated (such as dust or sea salt) and have larger sizes [1]. A spectrally invariant, homogenous, complex refractive index is also specified for each size mode. Using these eight parameters (r_e, v_e and complex refractive index for each size mode), multiple scattering is calculated using the doubling and adding method [29, 30] and a measure of aerosol loading for each mode. We use the layer AOT at 560nm to specify load. The number of aerosols in a volume can be computed with this AOT and the aerosol extinction coefficient, which is uniquely specified by the aerosol size and refractive index. In this study, aerosols are placed in the planetary boundary layer, and have a maximum height of 1km. Versions of this radiative transfer software package have been in use at the NASA Goddard Institute for Space Studies for many years now, e.g. [19–21].

In addition to parameters describing aerosol optical properties, we must also find a way to succinctly describe surface reflectance. Ocean reflectance is calculated using the method originally discussed in [18], which was recently refined [32]. We use a "Case I" type of ocean, which means that phytoplankton particles are the dominant source of scattering, and a wind speed driven surface roughness as in [33]. In these conditions, ocean reflectance can be described with two parameters: Chlorophyll-a concentration (indicating phytoplankton) and wind speed. For simulations of an aerosol over the ocean, $\mathbf{x}$ contains twelve parameters, where ten are used to describe aerosol conditions (AOT, r_e, v_e and complex refractive index for each size mode), and two to describe the surface.

Simulations over land require a greater number of parameters. For total (non-polarized) reflectance, we parameterize the surface Bidirectional Reflectance Distribution Function (BRDF) (which defines the angular distribution of reflectance, [34, 35]) using the Ross-Li BRDF kernel models. This is similar to the approach used by the NASA Moderate Resolution Imaging

#172897 - $15.00 USD Received 19 Jul 2012; revised 24 Aug 2012; accepted 25 Aug 2012; published 4 Sep 2012

Spectroradiometer (MODIS) instruments [36–38] and has previously been used with scanning polarimeters in [39]. This method uses three parameters as scaling coefficients to a BRDF. The Volumetric BRDF kernel represents scattering within a dense vegetation canopy, while the Geometric kernel is representative of surfaces with larger gaps between objects and therefore accounts for self shadowing. The Isotropic kernel is a uniform reflectance at all angles. Combinations of these three kernels can represent most surface BRDF's, at least for view angles common to orbital remote sensing instruments [38]. Furthermore, the Volumetric and Geometric kernels show little spectral variation for visible and near-infrared wavelengths [40, 41], so a single value of each can describe that component of the BRDF for all observed wavelengths. The Isotropic kernel is typically spectrally dependent, so we must select a unique value for each wavelength. Since our simulations include polarization, we must also describe the Polarized Bidirectional Reflectance Distribution Function (pBRDF). Because polarization generally involves interactions with the front facet of a surface, the pBRDF is spectrally invariant, and has an angular dependence similar to the Fresnel reflectance [11, 42–44]. For this BRDF component, we simply scale the Fresnel reflectance coefficient, cf. [21]. For simulations of aerosols over land, $\mathbf{x}$ therefore contains ten parameters describing aerosols, three parameters for the spectrally invariant portions of the BRDF and pBRDF (the Volumetric and Geometric kernels and the scaling term for the Fresnel reflectance coefficient), and a parameter for the Isotropic reflectance kernel at each observed wavelength. For an instrument with seven spectral channels, $\mathbf{x}$ has twenty parameters.

2.4. Simulation specifics

In order to make our results representative of variable global conditions, we have simulated several types of aerosols, at different concentrations, suspended in a standard atmosphere over two types of surfaces (land and ocean). The goal is to make this simulation as realistic as possible for global remote sensing, since disparate aerosol and surface conditions have different estimated uncertainties. The focus of this work is the retrieval of fine size mode dominated aerosols, while coarse size mode aerosols will be examined in a subsequent analysis.

For aerosol properties, we use data from the Aerosol Robotic Network (AERONET) [45]. An assessment of AERONET data is described in [46], where several sites associated with particular aerosol types are considered. We use the mean optical properties of six of these sites as our simulated aerosol properties. Because this analysis uses spherical particles, we exclude classes associated with non-spherical aerosols, such as dust. We also exclude classes associated with coarse size mode aerosols, such as sea salt. Future work will involve the incorporation of non-spherical aerosol models that have been identified as compatible with various airborne polarimetric observations [32]. Table 1 contains the aerosol microphysical properties used for this study, along with other model details. These parameters are reported in Dubovik et al. [46], although for consistency with our radiative transfer model, we tabulate the effective variance [29] rather than the log standard deviation of the size distribution. Dubovik et al. report that size parameters are weak functions of AOT, but for simplicity we use the parameters associated with the mean reported optical thickness for all our simulations. All simulations are dominated by the fine size mode, which contributes 90% of the total AOT at 560nm. Furthermore, the refractive index is identical for both fine and coarse size modes, which is probably not realistic since the modes are generated by different processes. Since we lack further information on complex refractive index for this assessment, we use this simplification in our simulation.

As we shall see in the results, simulated retrieval error can be highly dependent upon AOT. Generally, uncertainties decrease as AOT increases, since it is easier to retrieve aerosol optical properties when more of those aerosols are present. For this reason, it is important to choose AOTs that are a realistic representation of global conditions. We use the AOT from the

#172897 - $15.00 USD Received 19 Jul 2012; revised 24 Aug 2012; accepted 25 Aug 2012; published 4 Sep 2012

Table 1. Aerosol microphysical properties used in this study, based upon AERONET climatology [46]. All classes are composed of spherical, homogenous particles with a spectrally invariant refractive index. Size is specified bimodally with lognormal distributions. The fine size mode dominates scattering for each class, and contributes 90% of the total AOT at 560nm.

Site or type	**Refractive index**	$r_{e,fine}$ [μm]	$v_{e,fine}$	$r_{e,coarse}$ [μm]	$v_{e,coarse}$
Amazon Forest	$1.47 - i0.001$	0.176	0.174	6.91	0.867
African Savanna	$1.51 - i0.021$	0.152	0.174	5.95	0.704
Paris, France	$1.40 - i0.009$	0.173	0.203	5.39	0.867
Greenbelt, MD, USA	$1.40 - i0.003$	0.170	0.155	5.52	0.755
Mexico City, Mexico	$1.47 - i0.014$	0.165	0.203	4.43	0.487
Maldives	$1.44 - i0.011$	0.222	0.236	4.96	0.782
Model Configuration					
Solar Zenith Angle: 45°, Relative Azimuth Angle: 45°					
Aerosols vertically distributed uniformly between the ground and 1km					
Fine mode aerosol fraction of AOT(560nm): 90%					
Simulated at AOT(560nm): 0.039, 0.084, 0.123, 0.181, 0.346					
Ocean: Windspeed: 5m/s, Chlorophyll-a: 0.1mg/m^3					
Land: Bare soil with broadband bihemispherical reflectance of 0.177 (see [39])					

OsloCTM2 global aerosol-chemisty transport model for this purpose, since this model is proven to accurately predict the aerosol direct radiative forcing [47], and because a global model is less sensitive to the potential for spatial and temporal sampling biases of satellite observations. While the model simulates AOT at 550nm, we use this value in our simulations for AOT at 560nm, and assume the differences are negligible (no more than 0.01 in AOT). The OsloCTM2 is an off-line model driven by meteorological data that compares well to ground and satellite observations [47]. Figure 1 is the AOT histogram from OsloCTM2, along with the Cumulative Distribution Function (CDF). Green bars indicate the centroids of the distribution quintiles, which are the values chosen for simulation in this study. Note that the AOT is log-normally distributed, with a long tail and the middle quintile value slightly larger than the distribution peak.

Surface reflectance and other model characteristics are shown in Table 1. A nominal, midlatitude spring or fall viewing geometry (for the APS) was chosen, along with an ocean surface representing typical open ocean conditions with moderate wind. The (total and polarized) reflectance for such an ocean was computed following [32]. Land surface reflectance comes from the "soil" class in [39]. The impact of gaseous absorption is neglected. For real observations, such as those from RSP for the 1600 and 2250nm spectral bands, this effect is easily corrected because the carbon dioxide and methane absorption can be modeled as a two pass transmission correction combined with a small absorption optical thickness in the aerosol layer [39, 48].

2.5. Measurement error covariance matrix

The measurement error covariance matrix, $\mathbf{S}_\varepsilon$, describes observation uncertainty. Diagonal terms of the covariance matrix represent the squared uncertainty in an individual measurement, while off diagonal terms represent correlation in the error between pairs of measurements.

Individual measurement uncertainties vary for different observation types, as described below. Simulations are for instruments that are sensitive to polarization and we use the Stokes polarization vector, [29]

#172897 - $15.00 USD Received 19 Jul 2012; revised 24 Aug 2012; accepted 25 Aug 2012; published 4 Sep 2012

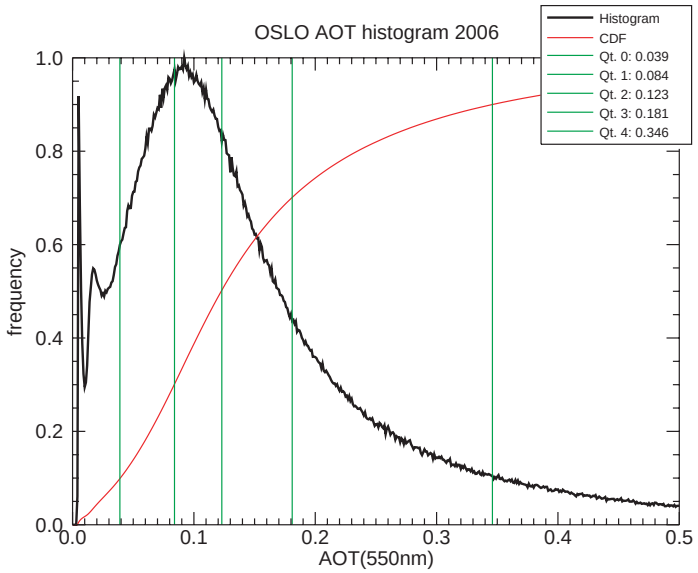

Fig. 1. Global AOT at 550nm for 2006 from the OsloCTM2 model. The histogram is shown in black, while the Cumulative Distribution Function (CDF) is in red and distribution quintiles in green. This histogram was used to select the appropriate simulation AOT, where the centroid of each quintile was used as the simulation AOT.

$$\mathbf{I} = [I, Q, U, V]^T, \tag{5}$$

to represent the state of polarization of the scattered light, where Q and U indicate the direction and magnitude of linearly polarized intensity, V the circular polarization, and I the total intensity, with units of $\mathrm{Wm}^{-2}\mathrm{sr}$. Circular polarization is minimal for observations of the atmosphere [49], and is therefore neglected in the following analysis. We prefer to work in units of reflectance, so that all bands have a similar dynamic range, and we define this for each relevant Stokes vector element to be

$$R_I = \frac{I\pi r_o^2}{F_o \cos\theta_s}, \qquad R_Q = \frac{Q\pi r_o^2}{F_o \cos\theta_s}, \qquad R_U = \frac{U\pi r_o^2}{F_o \cos\theta_s}, \tag{6}$$

where F_o is the annual average exo-atmospheric irradiance ($\mathrm{W/m}^2$), r_o is the solar distance normalized by the average sun-earth distance (thus compensating for solar distance deviation from average throughout the year), π is used to relate radiant intensity to irradiance (and has the unit of sr^{-1}), and θ_s is the solar zenith angle. Most polarization information can be contained within a single parameter, the polarized reflectance

$$R_p = \sqrt{R_Q^2 + R_U^2}, \tag{7}$$

so in many cases observations are in units of R_I and R_p, representing the total and polarized reflectances, respectively. In some cases, the Degree of Linear Polarization ($DoLP = R_p/R_I$) is a better measure of polarization, since as a relative measurement it is more accurate. Over the ocean, we use the $DoLP$ because the total reflectance of the open ocean varies systematically

#172897 - $15.00 USD Received 19 Jul 2012; revised 24 Aug 2012; accepted 25 Aug 2012; published 4 Sep 2012

with Chlorophyll concentration. Over land, the spectral invariance of the surface polarized reflectance means that it is usually chosen as the measurement unit, since it is not affected by surface spectral albedo variation [12, 21, 43]. In Section 3.4 we investigate this issue by comparing retrievals over land that only use R_p to those that use both R_I and *DoLP* (but need to constrain more parameters). We should also point out that *DoLP* used here is always positive, but an alternate version is $DoLP = -Q/I$ for $U = 0$ [50]. While we do not use this version in the current study, it presumably contains slightly more information than the unsigned *DoLP*.

Our measurement error covariance matrices therefore contain uncertainties for R_I, and R_p or *DoLP*. Each of these have contributions from shot noise (and other instrumental artifacts), calibration, and polarimetric characterization effects. These uncertainties (for APS) are

$$\begin{aligned}
\sigma_{R_I}^2 &= 2\sigma_f^2 \left(\frac{\pi r_o^2}{F_o cos(\theta_s)}\right)^2 + \sigma_a \frac{R_I \pi r_o^2}{F_o \cos\theta_s} + \sigma_b^2 R_I^2, \\
\sigma_{R_p}^2 &= 2\sigma_f^2 \left(\frac{\pi r_o^2}{F_o cos(\theta_s)}\right)^2 + \sigma_a \frac{R_I \pi r_o^2}{F_o \cos\theta_s} + \sigma_b^2 R_p^2 + \sigma_c^2 R_p^2, \\
\sigma_{DoLP}^2 &= 2\sigma_f^2 (1+DoLP^2) \left(\frac{\pi r_o^2}{R_I F_o cos(\theta_s)}\right)^2 + \sigma_a (1-DoLP^2) \frac{\pi r_o^2}{R_I F_o \cos\theta_s} + \sigma_c^2 DoLP^2.
\end{aligned} \tag{8}$$

The parameters σ_f, σ_a, σ_b, and σ_c define the amount of uncertainty due to different components of the system, and vary for each instrument design. σ_f is uncertainty due to instrument dark current noise (the "floor"), while σ_a describes the instrument shot noise. Both of these uncertainties are considered random, and therefore only contribute to the diagonal of $\mathbf{S}_\varepsilon$. For typical APS uncertainties of scenes of aerosols above a dark surface, dark and shot noise contribute minimally to the total uncertainty for σ_{R_I} and σ_{R_p}. Dark and shot noise are a large portion of the total uncertainty for σ_{DoLP}, at least when polarimetric uncertainties are small as is the case for APS. σ_b is the radiometric calibration uncertainty. We use 3% for all instruments. For σ_{R_I} and σ_{R_p}, calibration uncertainty is usually the largest contribution to total uncertainty. This is the reason observations of *DoLP* are preferable, since σ_{DoLP} is insensitive to uncertainty in the absolute radiometric calibration. σ_c represents the uncertainty in polarimetric calibration associated with small values of *DoLP* (the relative gain of channels measuring orthogonal polarization states). These values vary for different instrument types, as described in detail in section 2.7. For instruments similar to APS, σ_c can have values as low as 0.2% [51].

The above uncertainties are the individual values for each measurement, and form the diagonal of $\mathbf{S}_\varepsilon$. Off diagonal terms indicate the correlation between the uncertainty of pairs of measurements. For example, a calibration related bias because of an optical component in the sensor might affect some portion of m uniformly. In this work, we assume that dark and shot noise (represented by σ_f and σ_a) are uncorrelated, while all other sources of uncertainty may be correlated for various viewing angle measurements of the same polarization state and spectral channel. We simulate this correlation with a Markov process, using

$$\begin{array}{ll}
S_{\varepsilon,i,j} = \sigma_i^2 & \text{for } i = j, \\
S_{\varepsilon,i,j} = \sigma_{c,i}\sigma_{c,j}\rho^{|a(i-j)|} & \text{for } i, j \text{ in the same channel and polarization state}, \\
S_{\varepsilon,i,j} = 0 & \text{otherwise},
\end{array} \tag{9}$$

where ρ is the correlation parameter that describes the degree of correlation, and a is the view angle separation between adjacent observations. $\sigma_{c,i}$ is the portion of σ_i that is due to correlated uncertainties (terms on the right hand side of Eq. (8) that include σ_b and σ_c). For example,

#172897 - $15.00 USD Received 19 Jul 2012; revised 24 Aug 2012; accepted 25 Aug 2012; published 4 Sep 2012

$\sigma_{I,c}^2 = \sigma_b^2 R_I^2$. A value of zero for ρ denotes no correlation, while 1 means full correlation. This is raised to a power equal to the angle between i and j. This means correlation will be greatest for adjacent measurements, and fall off as the distance between them increases. $\mathbf{S}_\varepsilon$ is therefore a block diagonal matrix if $\mathbf{y}$ contains multiple channels or polarization states, and ρ is nozero.

The degree of correlation (ρ) is difficult to determine for most instrument systems. For instruments such as APS, which observe a scene at about 250 viewing angles, a high degree of angle to angle correlation can be expected for uncertainties due to polarimetric and radiometric calibration coefficients. This is because adjacent observations involve nearly identical optical interactions. The impact of this correlation depends upon the type of measurement. As described above, the *DoLP*, which is a ratio of two observations, is less sensitive to calibration uncertainty, and therefore has less correlation dependence. The largest uncertainties in R_I and R_p, however, are due to calibration, so those observations are impacted by the degree of uncertainty correlation. The effect of this on the overall information content is shown in Fig. 2. In this Fig., the SIC for an urban aerosol (Greenbelt, MD, USA, see Table 1) over water at an optical thickness of $\tau(560\text{nm}) = 0.123$ is determined for an APS type instrument with various error correlations and number of viewing angles. Solid lines indicate the information contained within the *DoLP* only, while dashed lines show the information in R_I alone. Color indicates the number of viewing angles used, while all other instrument properties (such as spectral bands) are identical to the APS. The simulated scene changes slowly with respect to viewing angle, and is probably well represented with as few as 16 view angles (other scenes, such as warm phase clouds, can have much more structure with respect to view angle). Therefore, more viewing angles primarily reduce the random uncertainties due to shot and dark current noise. Improvement due to this lessens as the correlation of calibration uncertainties increases. Furthermore, since R_I is more sensitive to correlated errors than *DoLP*, this decrease is more relevant for total (and polarized) reflectance. In this study, we arbitrarily choose to use $\rho = 0.9$ as our correlation parameter, because we expect a large amount of calibration uncertainty correlation and it is the worst case scenario for information content reduction for R_I and R_p. As we can see from Fig. 2, using many viewing angles still improves the SIC when using a large correlation, although this improvement is much more dramatic for *DoLP* than for R_I. We therefore show that while APS was designed with many view angles in order to capture warm phase cloud features, this instrument configuration can also reduce uncertainties for scenes that do not vary rapidly with respect to angle. This result is somewhat different from that derived in [27], because in that study uncertainties were not split into correlated and uncorrelated components.

2.6. The a priori error covariance matrix

The *a priori* error covariance matrix, as we use it here, defines the knowledge of atmospheric and surface parameters prior to measurement. We know, for example, the global distribution of AOT (see Fig. 1), so we expect the AOT in our scene to generally fall within this range. The act of making a measurement enhances our knowledge of some parameters, and the result is expressed in the retrieval error covariance matrix. The reduction in uncertainty for all parameters is shown in the SIC, while the reduction in uncertainty for specific parameters indicates measurement sensitivity. Practically, the *a priori* error is difficult to define numerically. We base $\mathbf{S}_a$, in an *ad hoc* manner, on the histogram of AOT values from the OsloCTM2 model [47] (see Fig. 1) and the AERONET based climatologies of [46]. The primary goal of this study is to compare the relative merit of different instrument designs, so that perfect *a priori* uncertainties will not be necessary, as long as they are reasonable and uniform for the various instrument designs. Table 2 lists the *a priori* uncertainties we chose for this study, where uncertainties are half the range of models presented in Table 1, and their squares becomes the diagonals in $\mathbf{S}_a$ (we assume no prior parameter correlation).

#172897 - $15.00 USD Received 19 Jul 2012; revised 24 Aug 2012; accepted 25 Aug 2012; published 4 Sep 2012

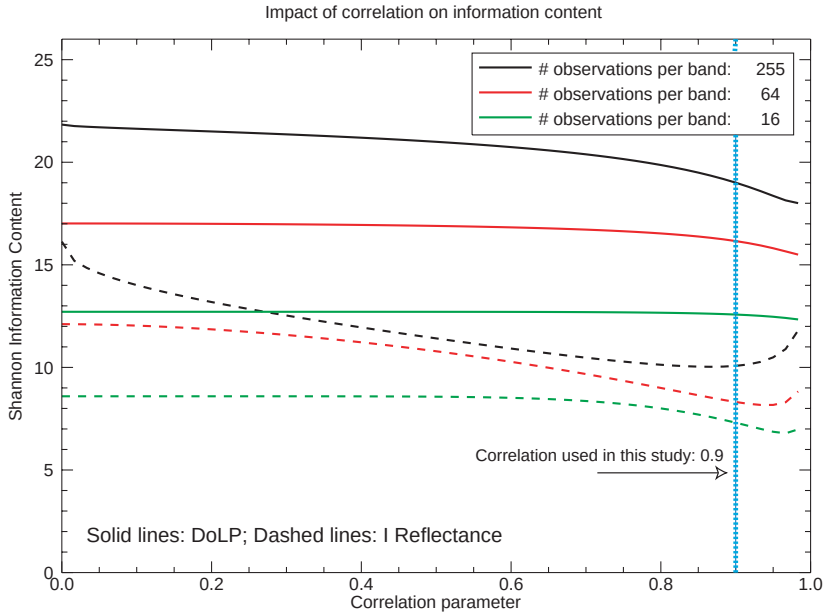

Fig. 2. The relationship between the Shannon Information Content (SIC) and error correlation parameter, ρ (see Eq. (9)) is shown for a simulation of an urban aerosol ($\tau(560nm) = 0.123$) over water for various instrument view angle configurations. Solid lines indicate the SIC contained in the *DoLP*, while dashed lines are for R_I. Overall, increases in ρ cause a decrease in the information content, except for extremely large correlations for R_I. This relationship is strongest for R_I, while the *DoLP* is much less sensitive to increased uncertainty correlation. This is because σ_{DoLP} is dominated by random noise, and means that instruments with large numbers of viewing angles can successfully increase the SIC even if the scene itself does not change dramatically with viewing angle. This is illustrated by the significant *DoLP* SIC differences for different viewing angle configurations when ρ is large, compared to much more modest differences for R_I. In this simulation, spectral bands and uncertainties are identical to the APS instrument, as described in Table 3.

Table 2. *a priori* error covariance matrix values

Size mode	**AOT**	**Refractive index**	r_e [μ m]	v_e
Fine	0.154	$0.075 - i0.01$	0.035	0.043
Coarse	0.154	$0.075 - i0.01$	1.310	0.190

Surface Parameters

Ocean: Windspeed: 2.5 [m/s], Chlorophyll-a: 0.5 [mg/m^3]

Land: Fresnel: 0.5, Volumetric: 0.2, Geometric: 0.02
Isotropic: 0.05 (for each channel)

#172897 - $15.00 USD Received 19 Jul 2012; revised 24 Aug 2012; accepted 25 Aug 2012; published 4 Sep 2012

2.7. *Simulated instrument designs*

To place this sensitivity study in the context of the current aerosol remote sensing capability, we present our results for three current or planned instrument designs. All of these instruments combine multi-angle and multi-spectral observations, and two of the three are also sensitive to the polarization state. Single view instruments, such as the MODerate resolution Imaging Spectroradiometer (MODIS) [52–55] cannot be included in a study such as this because there are fewer observations than there are parameters to retrieve. Single view angle systems are therefore numerically underdetermined, which means that $\hat{\mathbf{S}}$ would include an implicit regularization. In other words, this simulation would show an unrealistically low uncertainty for those instruments. Instead, we only simulate sensors that make more observations than retrieved parameters.

Table 3. Simulation instrument configurations for MISR, PARASOL and APS. The value in parentheses is the total number of measurements by each instrument for a scene location.

	Accuracy[#]	**Channels** [nm]		
Instrument	Polarimetric	Radiometric	Polarimetric	Angles
MISR (36)	σ_c : n/a	4: 440-870	none	$9 : \pm 70^\circ$
PARASOL (144)	σ_c : 0.01*	6: 440-1020	3: 490-870	$16 : \pm 55^\circ$
APS (224)	σ_c : 0.002	7: 410-2250	7: 410-2250	$255 : \pm 60^\circ$

* Over water, $\sigma_c : 0.02$ over land. See Eq. (10) for details.
[#] Radiometric accuracy, dark current and shot noise are held constant for all designs, with: $\sigma_f : 7 \times 10^{-5}, \sigma_a : 7 \times 10^{-8}, \sigma_b : 0.03$.

The first simulated instrument is based upon MISR, launched in 1999 on the NASA Terra spacecraft, and making observations of R_I in four channels at nine view angles [56–58]. Those four channels are centered at 446, 558, 672 and 866nm, but for consistency with other instruments, we simulate them at monocromatic wavelengths of 440, 560, 670 and 870nm. MISR observes each scene at nine view angles, with one at nadir and others at 26.1°, 45.6°, 60.0°, and 70.5° in both the forward and aft directions of the satellite track, and we simulate this angular distribution in the same manner. Post-launch relative radiometric calibration uncertainty is reported at $\sigma_b = 3\%$, with 1% channel to channel correlation [59]. For consistency with other instruments, we neglect the channel to channel correlation, but this would presumably reduce the information content of these measurements.

The next simulated instrument is POLDER, flown as part of the PARASOL mission [60]. Earlier versions of POLDER were launched in 1996 and 2003, but only survived for several months each due to spacecraft problems. The third POLDER (which we will refer to hereafter by its mission name, PARASOL, to distinguish it from the earlier instruments which had slightly different characteristics) was launched in 2004 by the Centre National d'Études Spatiales (CNES). PARASOL was a part of the "A-Train" constellation of satellites until 2011 [61], although it is now in a different polar orbit due to the depletion of fuel required to maintain position within the A-Train. This instrument has channels centered at 443, 490, 565, 670, 763, 765, 865, 910, 1020nm, but we simulate only aerosol retrieval relevant wavelengths of 440, 490, 560, 670, 870, 1020nm. Three of these channels, 490, 670 and 870nm, are sensitive to linear polarization by the use of a filter wheel. POLDER makes observations at a maximum of sixteen view angles per pixel between 55° forward and aft of the satellite track [62]. We use a radiometric calibration uncertainty of $\sigma_b = 3\%$ and polarimetric uncertainty of $\sigma_c = 1\%$ [63–65] over dark, homogenous surfaces such as water. Over land, we use $\sigma_c = 2\%$. This instrument does not

#172897 - $15.00 USD Received 19 Jul 2012; revised 24 Aug 2012; accepted 25 Aug 2012; published 4 Sep 2012

make simultaneous measurements (since a filter wheel is used to observe different polarization directions), so we apply a slightly different polarimetric uncertainty characterization than in Eq. (8), where σ_{R_I} is unchanged and σ_{R_p} and σ_{DoLP} become.

$$\begin{aligned}\sigma_{R_p}^2 &= 2\sigma_f^2\left(\frac{\pi r_o^2}{F_o cos(\theta_s)}\right)^2 + \sigma_a\frac{R_I\pi r_o^2}{F_o\cos\theta_s} + \sigma_b^2 R_p^2 + \sigma_c^2 R_I^2,\\ \sigma_{DoLP}^2 &= \sigma_f^2(1+DoLP^2)\left(\frac{2\pi r_o^2}{R_I F_o cos(\theta_s)}\right)^2 + \sigma_a(1-DoLP^2)\frac{\pi r_o^2}{R_I F_o\cos\theta_s} + \sigma_c^2,\end{aligned} \tag{10}$$

The impact of these changes, and the increase in polarimetric uncertainty (σ_c), means that σ_{DoLP} is dominated by correlated calibration uncertainties rather than uncorrelated dark and shot noise uncertainties.

Finally, the third simulated instrument is a design similar to the APS. The APS was an instrument on the NASA Glory satellite, that failed at launch in 2011. While the future of this instrument remains uncertain, we compare it here because it represents a different observation philosophy than previous instruments. The APS, which observes a single-pixel-wide swath, sacrifices global coverage in order to maximize the information content available in each measurement. The objective is to complement the existing data set from imaging instruments such as MODIS, MISR and POLDER by providing highly accurate aerosol properties for comparison with the simulation of aerosols in General Circulation Models (GCMs) [5, 13]. In this sense, APS can be considered a bridge between the coverage of imaging instruments and the accuracy of ground based networks such as AERONET. The APS had nine spectral channels centered at 413, 444, 555, 674, 866, 911, 1376, 1603 and 2260nm [51], of which seven are relevant for aerosol retrievals. We simulate the aerosol relevant channels at 410, 440, 560, 670, 870, 1600 and 2250nm. All of these channels are sensitive to linear polarization by the use of Wollaston prisms, thus ensuring simultaneous measurements of orthogonal wave oscillations and allowing for a significantly higher accuracy than the filter wheel approach. Preflight radiometric calibration uncertainty was found to be no greater than $\sigma_b = 3\%$ for visible channels (slightly higher for near-IR channels, but no more than 5.2%), while relative polarimetric uncertainty was between $\sigma_c = 0.08\%$ and 0.15% for different channels [51]. For simplicity, we simulate all channels with an uncertainty of $\sigma_b = 3\%$, $\sigma_c = 0.2\%$. The APS had 255 view angles in a scan from about 60° forward and aft of the satellite track.

Table 3 summarizes the three instrument designs used in this study. We also note that spatial resolution differences are not included. APS spatial resolution was to be 5.6km at nadir, while PARASOL is 5.3x6.2km and MISR is 1.1km (although MISR and level 2 PARASOL aerosol data products are averaged to a spatial resolution of 17.6km and 18.5km, respectively). Conceivably, a higher spatial resolution instrument could be compared to a lower resolution instrument by adding to the measurement vector, *m*, until both instruments represent the same ground footprint. These additional measurement vector elements would have highly correlated errors, with an impact similar to what is shown in Fig. 2. Considering that lower spatial resolution instruments (APS and PARASOL) have more angular views than the higher spatial resolution instrument (MISR), the need to account for spatial resolution is inconsequential for comparative purposes.

3. Results

In this paper, we compare three instrument designs for the remote sensing of fine size mode dominated aerosols. The simulated uncertainty for each aerosol (or surface) parameter retrieval is compared for two scenes (one over land, the other over water, see Table 1). The first scene is that of boundary layer aerosols over a deep ocean with moderate Chlorophyll-a concentration

#172897 - $15.00 USD Received 19 Jul 2012; revised 24 Aug 2012; accepted 25 Aug 2012; published 4 Sep 2012

and wind speed, while the second represents the same aerosols over a recently plowed field. Viewing geometry is identical in both, and represents what an instrument in a polar orbit would observe in the spring or fall in the midlatitudes.

3.1. Individual aerosol model results

We compared instruments using an assemblage of aerosol simulations, representing the optical properties expressed in Fig. 1 and Table 1. We first assess the variability of results for these different simulations, so that we can understand the importance of our choice of aerosol models and their impact on simulated uncertainty. Figure 3 presents the results for each parameter for an APS observation (see Table 3) over the ocean. In each panel, the abscissa is the simulation total optical thickness, while the ordinate axis is the simulated uncertainty for the parameter noted in the title. The lower right panel is the Shannon Information Content (see Eq. (4)) as a function of simulation total optical thickness. Generally, we can see that simulated uncertainties decrease as optical thickness increases, and that the SIC increases with optical thickness. This is reasonable because we expect our ability to determine aerosol microphysical properties to improve if more particles are present, although it appears that there is an uncertainty floor for large optical thickness. Exceptions to this rule are surface properties, which are obscured by increasing AOT, and the AOT itself. Presented as a relative error, however, AOT uncertainty decreases as the aerosol load increases. Coarse mode parameter uncertainties are the same or close to the *a priori* values (which are also listed for each parameter in the lower right of each panel), indicating that there is low sensitivity to those parameters. For context, uncertainties that do not meet accuracy requirements for climate modeling (as described in [5]) are shown as shaded yellow areas. Panels without shaded areas are either entirely within the requirements (as is the case for fine mode effective radius and variance) or represent parameters whose accuracy requirements were not described in [5], such as imaginary refractive index, fine and coarse mode AOT, and surface parameters.

Uncertainties depend much more strongly on AOT than they do on the properties of an individual aerosol model. Well retrieved parameters (those whose uncertainty is far below the *a priori* values), such as AOT for both modes, fine mode refractive index and effective radius, and surface parameters, all show little sensitivity to aerosol type. Coarse mode parameters are affected by the choice of *a priori* uncertainty and are thus not well constrained by the measurement. This was expected, since by design the coarse mode contributed minimally to the observed signal. The impact of this lack of sensitivity for a simultaneous retrieval of both size modes is included in the simulated uncertainties for all parameters. Fine size mode parameter uncertainties are reasonable, so constraining coarse mode microphysical properties more than the *a priori* values are not essential for these fine size mode dominated scenes.

Generally, the various aerosol types have similar uncertainties (at least for well retrieved parameters), although the Amazonian Forest class has an anomalously high SSA uncertainty. This is interesting since those aerosols have the lowest imaginary refractive index among all the simulated aerosols, but the uncertainties for imaginary refractive index for that class are consistent with other classes. This indicates that SSA uncertainty depends on the complex interaction of several parameters, and not just the imaginary refractive index.

To further explore the sensitivity of simulated uncertainty to the choice of aerosol model, we plotted the dependence of the SIC on the simulated parameters in Fig. 4. The SIC for APS, PARASOL and MISR are shown for the scene of aerosols over water. The top left panel shows how SIC increases with AOT, which is expected because there are more aerosols interactions in the atmosphere. This sensitivity is greatest for the instruments that utilize polarization (APS and PARASOL). The SIC for other parameters shows no obvious dependence on the simulated parameter value. This indicates that the AOT is the most important parameter to simulate in the

#172897 - $15.00 USD Received 19 Jul 2012; revised 24 Aug 2012; accepted 25 Aug 2012; published 4 Sep 2012

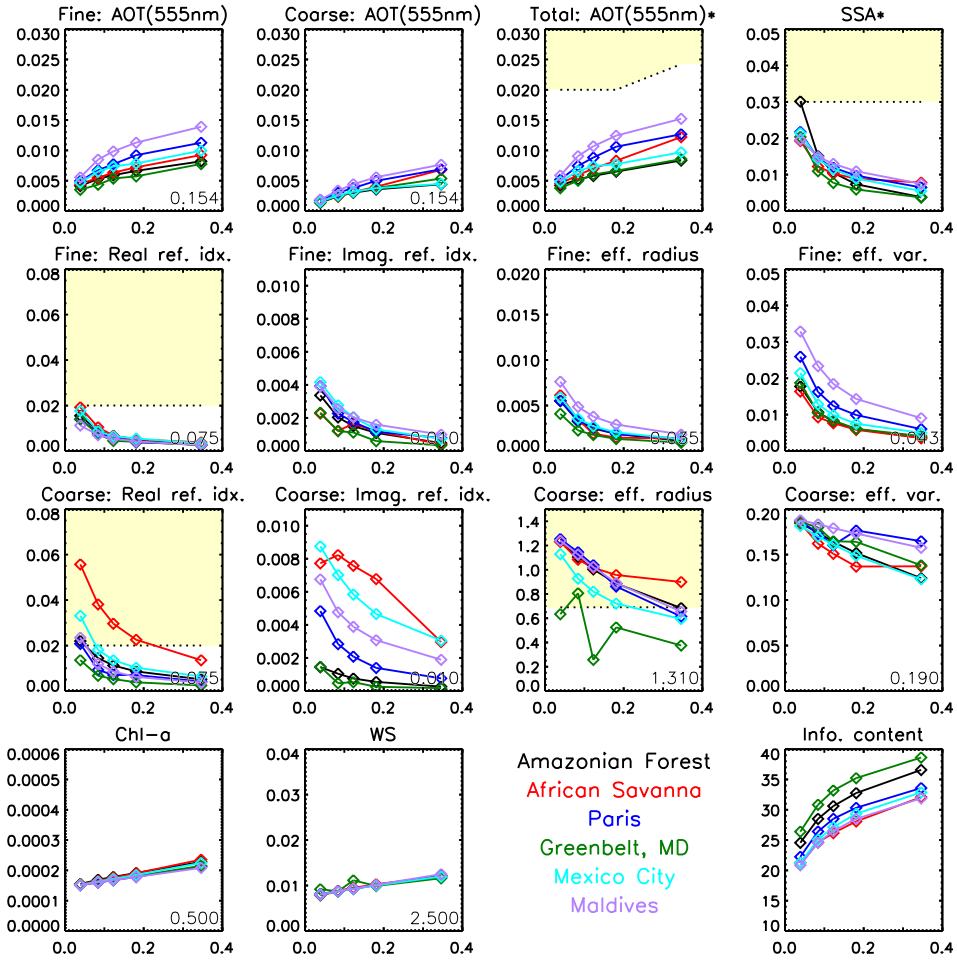

Fig. 3. Simulated uncertainties (components of $\hat{\mathbf{S}}$) for the APS for each aerosol climatology. The total simulated AOT values are the abscissae for each plot, while the ordinate axis is the simulated uncertainty. Shaded yellow areas indicate retrieval errors greater than the requirements in [5], while the *a priori* uncertainties for each parameter are in the lower right of each panel. The first row of plots contains the fine and coarse mode AOT and the (indirectly determined, as indicated by the *) total AOT and SSA. The second (third) row of plots are for the aerosol fine (coarse) size mode microphysical properties. The bottom row contains the surface parameter retrieval accuracies (Chlorophyll-a and wind speed) and the Shannon information content.

#172897 - $15.00 USD Received 19 Jul 2012; revised 24 Aug 2012; accepted 25 Aug 2012; published 4 Sep 2012

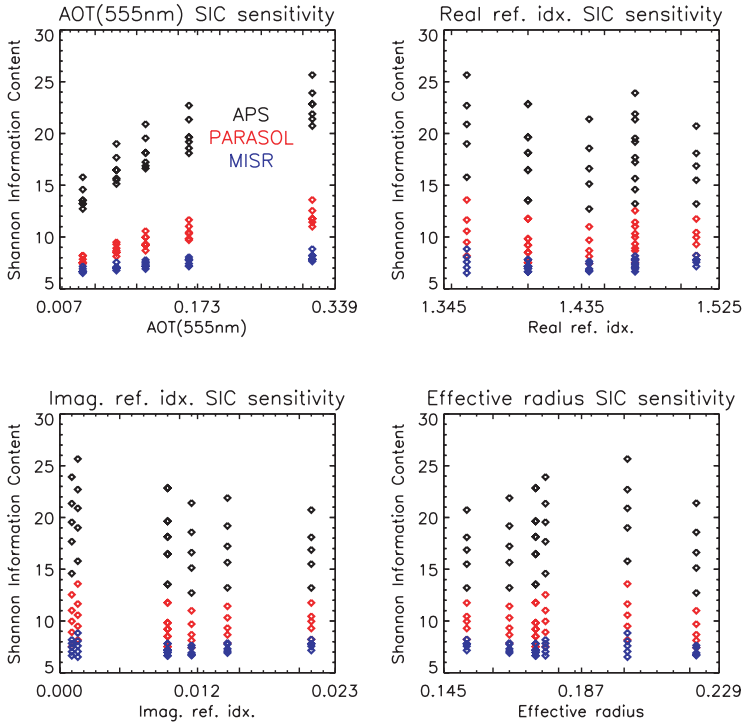

Fig. 4. This Fig. shows the sensitivity of the Shannon Information Content (SIC) to parameter variability among the simulated scenes. Many of the simulations share identical parameters (such as an individual aerosol type simulated at various AOTs), so the SIC value often has a large amount of scatter. This is less the case for the AOT, indicating that the AOT has a strong control on the information available in a scene. This means that in order for an assemblage of sensitivity studies to be globally representative, the selection of simulation AOT must be chosen with care, while other parameters are less important. Other parameters that are not shown here show a similar relationship, where microphysical aerosol optical parameters do not have a strong relationship with SIC.

#172897 - $15.00 USD Received 19 Jul 2012; revised 24 Aug 2012; accepted 25 Aug 2012; published 4 Sep 2012

radiative transfer model correctly if a study is to be globally representative, and the selection of aerosol microphysical properties is not overly important as long as they generally encompass the properties of global aerosols. Some aerosol sensitivity studies examine retrievals accuracies at much higher optical thicknesses than are common globally, indicating that their results may underestimate the global uncertainty.

3.2. Comparison for aerosols over ocean

Fig. 5 shows the mean simulated uncertainty for the instrument types described in section 2.7. Vertical bars indicate the standard deviation of simulated uncertainties for all the aerosol model types at that AOT. All other aspects of the Fig., such as the axes and their ranges, are identical to Fig. 3, although coarse size mode microphysical parameters have been omitted due to their minimal contribution to the top of the atmosphere signal for these fine size mode dominated aerosols. APS and PARASOL have smaller uncertainties than MISR, most likely due to sensitivity to polarization. Furthermore, APS has smaller uncertainties than PARASOL, because of a greater polarimetric accuracy and wider spectral range. All three instrument types are capable of retrieving accurate information about the fine mode aerosol size distribution, while they contain less information about complex refractive index. Except for the lowest simulated AOT, the APS is capable of meeting accuracy criteria in [5] for AOT, the fine mode real refractive index and SSA, while PARASOL is capable of meeting the SSA criteria for slightly higher AOT's. Accurate retrieval of surface parameters seems feasible for all three instruments, and is most accurate for APS due to greater information about aerosols.

3.3. Comparison for aerosols over land

Fig. 6 shows the mean simulated uncertainty results for aerosols over a recently plowed field. Compared to over water retrievals, uncertainty is worse for nearly all instruments and parameters. Except for the largest aerosol loads, APS still meets the accuracy criteria for AOT in [5], although those criteria are more relaxed over land. Interestingly, PARASOL AOT uncertainties degrade the most (compared to Fig. 5) over land, so that they are nearly identical to the relatively unchanged MISR uncertainty. This is specifically due to a reduction in the coarse mode AOT uncertainty, probably related to PARASOL's lack of longer wavelength polarimetric channels. The relatively lower MISR uncertainties compared to POLDER for AOT and SSA are somewhat confusing, since POLDER has polarization, more view angles, and a slightly wider spectral range. The one advantage that MISR has over POLDER is the wide angular range of observations, since MISR observes at 60° and 70.5° in the forward and aft directions, while the largest view zenith angle of POLDER is 55°. If this analysis is repeated without the 70.5° MISR observations, the uncertainties degrade so that they are worse than POLDER. This indicates that there is a significant amount of information at high view zenith angles. However, this study does not account for modeling uncertainties, so the uncertainty increase from inaccurate simulations (a distinct possibility at large view zenith angles) would not be represented here. In any case, the largest overall uncertainty impact for land retrievals compared to ocean retrievals appears to be for the retrieval of complex refractive index and the SSA. No instruments meet the accuracy criteria for SSA, although the APS approaches the value for large AOT. Simulated SSA uncertainties for medium and low AOT are large enough to be useless. This indicates that retrievals over land may require some form of regularization or external information input to constrain parameters within the accuracy criteria. For example, [63] uses information from adjacent pixels. Several factors cause this increased uncertainty. Retrievals over land require constraints on a larger number of surface parameters than those over water. For example, over water, 12 aerosol and surface parameters are constrained, while over land, 16 are required for MISR, 19 for PARASOL, and 20 for APS. Furthermore, required assump-

#172897 - $15.00 USD Received 19 Jul 2012; revised 24 Aug 2012; accepted 25 Aug 2012; published 4 Sep 2012

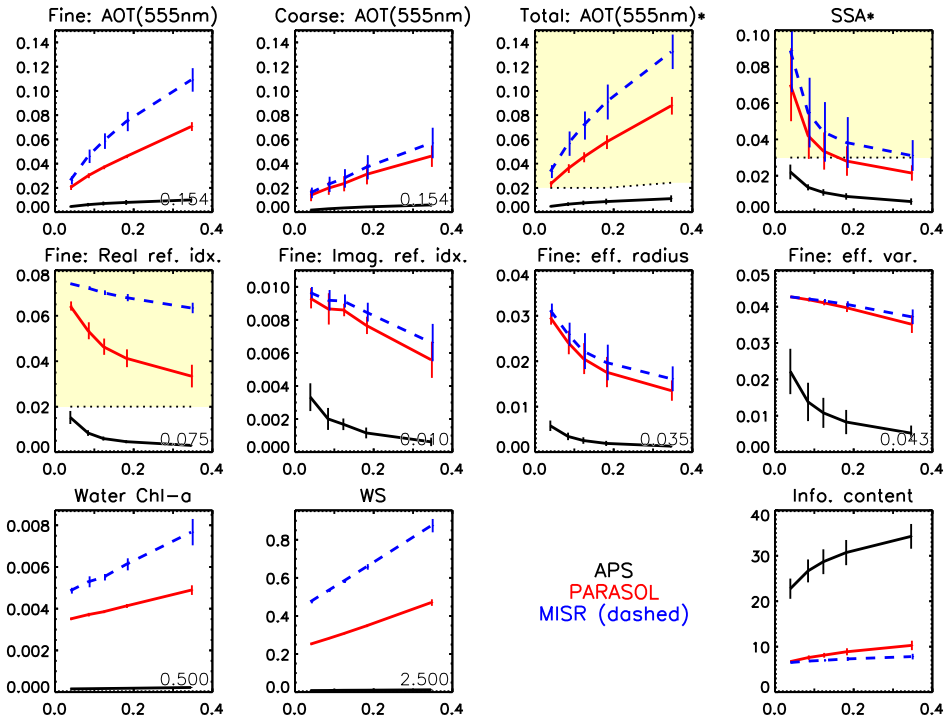

Fig. 5. Simulated retrieval uncertainty over the ocean for the instruments described in Table 3. The total simulated AOT values form the abscissae for each plot, while the ordinate axis is the simulated uncertainty. APS simulations are in black, PARASOL simulations in red, and MISR simulations in dashed blue. The axes range and other details of this Fig. are identical to Fig. 3.

tions about surface polarized reflectance (and the large value and spectral variability of the total reflectance) over land force the use of the polarized reflectance, R_p, rather than the Degree of Linear Polarization, *DoLP*. As we have seen in Eq. (8), the polarized reflectance uncertainty is dependent upon both the polarimetric accuracy, σ_c, and the radiometric accuracy, σ_b, whereas the *DoLP* is sensitive to polarimetric accuracy alone. For APS, the radiometric accuracy is often an order of magnitude worse than the polarimetric accuracy, so the polarized reflectance is significantly less accurate than the *DoLP*. In standard algorithms, however, R_p is used over land because of assumptions about the spectral invariance of the pBRDF. In the next section we test the wisdom of this approach by determining if other combinations of data have greater information content

3.4. Comparison of retrieval strategies for observations over land

In addition to outright comparisons of instrument designs, the analysis technique in this paper is an effective means to compare retrieval strategies. As an example of this, we compare various methods of retrieving aerosol parameters over land. As we have seen in section 3.3, retrievals of aerosols over land are less accurate than those over water. One of the primary reasons for this is the need to constrain additional parameters associated with the land surface BRDF. This raises the question of the use of total reflectance observations (R_I). The advantage of using the additional information contained within the total radiance observations may be outweighed

#172897 - $15.00 USD Received 19 Jul 2012; revised 24 Aug 2012; accepted 25 Aug 2012; published 4 Sep 2012

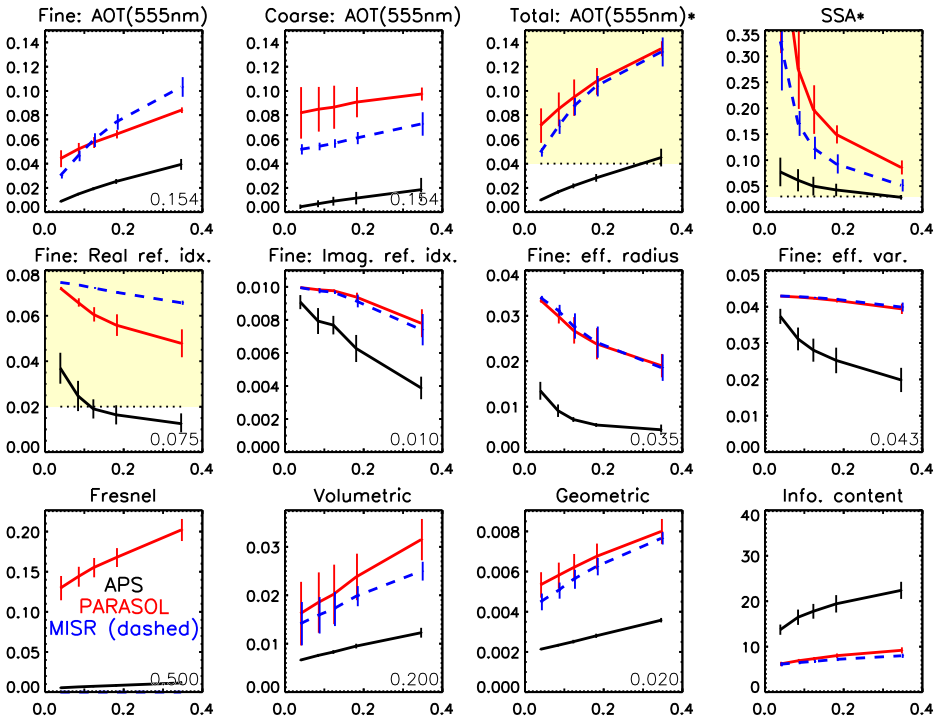

Fig. 6. Simulated retrieval uncertainty over land for the instruments described in Table 3. With the exception of the SSA range and surface reflectance kernels, the axes and other details of this Fig. are identical to those in Fig. 3.

by the need for the retrieval of additional parameters. Figure 7 compares retrievals that use polarized reflectance alone to retrievals that use both the total and polarized reflectance (or *DoLP*), but must also constrain additional parameters.

For APS, it appears that retrievals utilizing both the total reflectance and the *DoLP* are modestly superior, with *SSA* results now meeting uncertainty requirements for modest and large aerosol loads. The difference may be even greater if using the signed *DoLP*. This observational configuration is also feasible operationally, since the land surface *DoLP* can be determined from the ratio of the polarized to total *BRDF*. Interestingly, retrievals that use total and polarized reflectance contain the same amount of information about aerosols as retrievals that use polarized reflectance alone (and thus constrain fewer parameters). This means that whatever information contained within the total reflectance is entirely spent upon constraining the additional land surface parameters. The situation is drastically different for PARASOL, primarily due to the large polarimetric accuracy differences of APS and PARASOL. The use of total reflectance dramatically improves the quantity of aerosol information in a measurement, regardless of whether *DoLP* or polarized reflectance are included. For PARASOL, the less polarimetrically accurate *DoLP* is as valuable as the polarized reflectance (when combined with total reflectance), while for APS the increased *DoLP* accuracy means that it is worthwhile to work with data in that form when possible. These results are also consistent with [63], who found that better retrievals are possible if POLDER total reflectance observations are utilized in the retrieval algorithm.

#172897 - $15.00 USD Received 19 Jul 2012; revised 24 Aug 2012; accepted 25 Aug 2012; published 4 Sep 2012

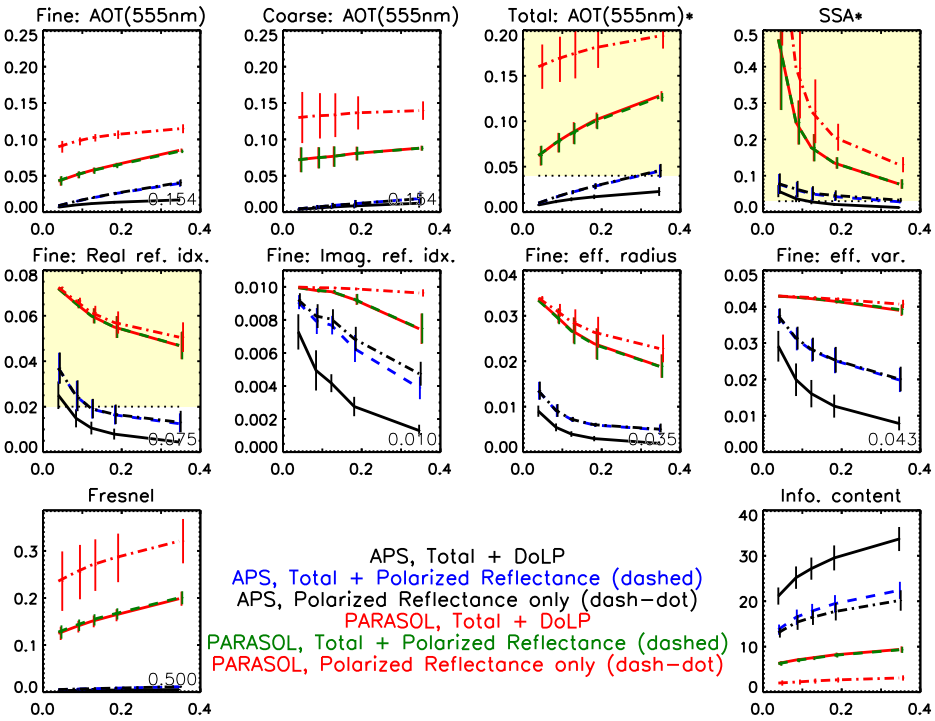

Fig. 7. In this Fig. we show the utility of various combinations of data for the retrieval of aerosol properties over land. Uncertainty for APS retrievals that use both total reflectance and the *DoLP* are plotted as black lines, total reflectance and polarized reflectance as blue dashed lines, and retrievals that use polarization alone (and therefore require the constraint of ten, rather than twenty, parameters) are plotted as dashed-dot black lines. PARASOL retrievals that use total reflectance and *DoLP* are plotted as red lines, total and polarized reflectance as dashed green lines, and polarized reflectance alone as red dashed-dot lines. While the axis ranges are different, all other parts of this Fig. are identical to Fig. 3.

4. Discussion

This paper describes a strategy to assess the information contained within a single (pixel) observation, based on the work of [25] and [26]. We use this method to compare the ability of three types of instruments to simultaneously retrieve aerosol properties over a (moderately dark) ocean or land surface, for a wide variety of aerosol types (from [46]) and AOT's (from [47]). As expected, the instrument designs that have access to polarization, make accurate measurements, and incorporate many spectral channels and view angles have lower retrieval uncertainties than alternate designs. In addition to comparisons, our results provide some idea of the absolute uncertainties one can expect for an instrument design. Of course, this method (like all sensitivity studies) is idealized, and does not account for uncertainties due to modeling error, retrieval algorithm problems, or other uncertainties not explicitly included in the error covariance matrix. Results are representative of a best case scenario, since we know that uncertainty cannot be lower unless additional information is provided (such as with more tightly constrained *a priori* parameter values or regularization methods). With this in mind, we compare our results to uncertainty assessments for these instruments in the literature. As we shall see, our results agree with previous studies of POLDER and APS sensitivities (with some exceptions, and only for

#172897 - $15.00 USD Received 19 Jul 2012; revised 24 Aug 2012; accepted 25 Aug 2012; published 4 Sep 2012

studies that use equivalent measurement uncertainty), but show generally larger uncertainties than have been predicted for MISR.

4.1. MISR

MISR aerosol retrievals have been assessed by many [66–73] and are partially summarized in [58]. In these studies, satellite retrieved AOT is compared to data collected by ground based observations such as AERONET. Most show that AOTs from MISR are found to be within 0.05 or $0.2 \times AOT$ of AERONET observations (other parameters are more difficult to compare). Minor exceptions are the findings of [68] ($\pm 0.04 \pm 0.18 \times AOT$). Comparison to AERONET is also a strategy used to assess uncertainty in MODIS optical thickness retrievals, and that instrument has been found to have a similar degree of agreement with AERONET [74–76]. However, biases have been found between MODIS and MISR that meet or exceed these accuracies [8, 9, 77], which casts doubt on one or both of those assessments. Our results also show that MISR AOT uncertainty exceeds the 0.05 or $0.2 \times AOT$ threshold for all aerosol simulations except those with the lowest optical thickness ($AOT(560nm) = 0.039$). While [8, 9] provide a more detailed insight into the sources of this problem, a primary concern is the need to constrain all the aerosol microphysical properties. Because of the limitations of the available information content in MISR observations (which are shown in our analysis by a low sensitivity to fine mode refractive index), the retrieval algorithm must utilize *a priori* assumptions about aerosol microphysical properties. The potential error of these assumptions is difficult to characterize, and is implicitly ignored when uncertainty assessments are based upon a comparison of a single parameter (AOT) alone. In other words, similar observations by MISR and AERONET may be due to incorrect assumptions about the aerosol microphysical properties, leading to a correct answer for the wrong reason. These results show that it is not possible for MISR to meet the 0.05 or $0.2 \times AOT$ AOT criteria based upon the information contained within the observation alone, and suggests that uncertainty due to assumptions about aerosol microphysical properties are underestimated.

4.2. POLDER/PARASOL

Our results are much more similar to published uncertainties for POLDER. There is a long history of retrievals from the POLDER instruments, but only two recent papers utilize all of the measurements to do simultaneous retrievals of aerosol and surface parameters. [64] uses a Phillips-Tikhonov regularization technique to retrieve aerosol microphysical properties over the ocean. Estimated uncertainties are also calculated in a manner very similar to this paper, and the results are comparable. Generally, we find lower uncertainties for fine mode aerosol parameters and higher uncertainties for coarse mode parameters, which is understandable considering that our simulated aerosols are dominated by the fine size mode. Total AOT uncertainties are lower (slightly more than half) than our simulated values. However, [64] also compares their results to AERONET retrievals, and the standard deviation of the differences between the two is nearly identical to our simulated uncertainty. SSA validation results also show nearly identical values to our simulated uncertainty. In addition, negligible sensitivity was found to coarse mode imaginary refractive index and effective variance, which agrees with our work. Over land, [63] uses a statistical optimization to retrieve aerosol properties by either using a single pixel of measurements or by using multiple adjacent pixels. The aerosol and surface parameters used in this work differ somewhat from our study, so comparisons are more problematic. However, they did test observations with biomass burning aerosols (the AERONET Mongu, Zambia site). Noise was added to the measurements to find the variability of the retrieved results. These noise levels were 1% for total reflectance, and 0.5% for polarized reflectance, which is a third and a quarter, respectively, of the uncertainty we used in our analysis. They found that SSA

#172897 - $15.00 USD Received 19 Jul 2012; revised 24 Aug 2012; accepted 25 Aug 2012; published 4 Sep 2012

uncertainty (at 440nm) varies between about 0.08 at the smallest AOT, to 0.04 at optical thicknesses that are equivalent to our maximum simulated values. This is significantly lower than our equivalent values of 0.3 to about 0.1, which we assume is due to the differences between their added noise and our simulated uncertainty. It could also be due to slight differences in the types of retrieved parameters in [63]. In a similar fashion, they found the AOT uncertainty to be about 20%, which is much smaller than our values, which range between 180% at the smallest simulated AOT, to 35% at the largest.

In conclusion, expectations of PARASOL retrieval uncertainty over the ocean largely agree with our results, as do validation against AERONET observations. Retrievals over land, performed with a slightly different set of aerosol parameters are more difficult to compare. Tests with lower quantities of noise than our simulations naturally find lower predicted uncertainty.

4.3. APS and RSP

Since the APS instrument was not successfully launched into orbit, there are no orbital data available for comparison. Fortunately, more than a decade of observations by the APS airborne prototype, the RSP, have been made during field campaigns throughout North America. Of these studies, [21] is most comparable to this work, and it involves simulations of fine mode dominated aerosols over a vegetated land surface. Their simulation study, which was methodologically equivalent to ours but used a different software implementation and aerosol simulation, finds remarkably similar results. For example, fine mode AOT uncertainties are within 0.003 of our predictions for a variety simulations at different total optical thicknesses. Similarities are also found for the coarse mode AOT, SSA, fine mode effective radius and the coarse mode real refractive index. Parameters to which the APS has lower sensitivity, such as fine mode effective variance, and coarse mode size, are more affected by *a priori* bounds. Since these were set slightly differently in [21] than is this work, predicted uncertainties were also slightly different. The largest differences are for the fine mode real refractive index, where [21] finds uncertainties between 0.01 and 0.015 larger than our results. That paper also compares actual retrievals to AERONET observations, and finds differences similar to the uncertainty predictions. Interestingly, the fine mode real refractive index comparison is better then the uncertainty prediction, and more similar to our findings. Another study assessed the RSP retrieval capability for an optically thick ($AOT(532nm) = 0.67$) smoke layer lofted in a vertically complex manner [19]. The retrieval method was somewhat different, since only one total reflectance channel (410nm) was used, and aerosol layer top height was retrieved, while surface reflectance parameters were not. Furthermore, aerosol amount was constrained with the number concentration parameter, rather than AOT, which was found to an unstable means to converge to a solution for high AOT scenes such as this. Understandably, this paper found larger uncertainties than we do, particularly for AOT and fine mode real refractive index. However, fine mode imaginary refractive index, SSA and effective radius are quite similar to our results. We interpret this to mean that our results are generally similar, since differences for AOT and fine mode refractive index are due to the use of aerosol number concentration (which co-varies with both AOT and fine mode refractive index) as the retrieval parameter.

While there are many analyses of RSP observations over water [14–16, 32], comparisons with these results are difficult. This is because those studies focus on specific aspects of the measurement sensitivity, and do not estimate overall uncertainty for retrieved parameters. [16] does compare RSP retrieved AOT to AERONET and an aircraft based sun photometer, and finds the retrieved values to be low by about 0.04 to 0.05 for moderately high aerosol loading of about $AOT(560) = 0.4$. This is slightly higher than our uncertainty estimates for retrievals of AOT over water, but that work also finds a large spatial and temporal AOT variability which accounts for some of the difference. In short, our simulated APS uncertainties for retrievals

#172897 - $15.00 USD Received 19 Jul 2012; revised 24 Aug 2012; accepted 25 Aug 2012; published 4 Sep 2012

over land agree very well with previous work. Fewer comparable results exist for retrievals over water, but those that do provide some support of our findings.

5. Conclusion

We present an analysis of the information content in multi-angle, multi-spectral and polarimetric observations for the retrieval of fine size mode aerosol and surface optical properties. This analysis has a narrowly defined scope, and is appropriate for remote sensing retrieval of boundary layer spherical aerosols dominated by the fine size mode. Radiative transfer is assumed plane parallel, and aerosol refractive indices are spectrally invariant. Otherwise, we attempted to replicate global observation conditions as much as possible by simulating six classes of aerosols observed by AERONET ground sun-photometers [46] at realistic optical thicknesses from the OsloCTM2 model [47]. This analysis method is ideally suited for the comparison of instrument designs, since it estimates retrieval uncertainty based solely on four simple instrument characteristics. These characteristics are the number and spectral distribution of observation channels, their polarimetric sensitivity, the number and range of view angle observations, and the accuracy of each of these measurements. Results are insensitive to the retrieval algorithm and other external factors (other than the *a priori* defined uncertainties). Because of the potential for modeling errors, real world retrievals are likely to be more uncertain than the results of this simulation. In that sense, this work identifies the best possible retrieval uncertainty, since we know that it is impossible to be more accurate without access to additional information about a scene.

Some of the major findings are listed below.

- Estimated uncertainty is strongly dependent upon the simulation AOT. This underscores the importance of performing sensitivity studies at realistic optical thicknesses, as in Fig. 1. On the other hand, estimated uncertainties are largely insensitive to changes in simulation optical properties, so it is reasonable to use a limited number of aerosol types for sensitivity studies.

- As expected, designs that have access to polarization, have a wide spectral and angular observation range, and are very accurate, are able to more accurately retrieve aerosol parameters in a scene than those that do not.

- Retrievals over land are less accurate than those over water, since more parameters must be constrained to describe surface reflectance and because of inherent differences in the uncertainty between the type of polarimetric information that are commonly used over land and ocean.

- Estimated uncertainties are similar to previous studies for the POLDER instrument and the RSP, an airborne prototype of the APS instrument. We find larger AOT uncertainties than have been previously reported for the MISR instrument. These differences are most likely due to an underestimation of the uncertainty due to aerosol microphysical property assumptions required for MISR retrievals, and may explain some of the differences that have been found between the MISR and MODIS instruments.

- Retrievals over land with the APS, which has a very low polarimetric uncertainty, do not benefit from the use of total reflectance observations, since they require additional constraints on surface reflectance. However, the less accurate POLDER instrument benefits from the use of total reflectance channels, particularly for the retrieval of AOT and SSA.

We intend to use this framework in the future for the investigation of retrieval strategies for other scenarios, such as mixed aerosol and cloud scenes and observations through ocean

#172897 - $15.00 USD Received 19 Jul 2012; revised 24 Aug 2012; accepted 25 Aug 2012; published 4 Sep 2012

surface glint. Additionally, the set of aerosol scenes will be expanded to include the coarse size mode and nonspherical particles.

Acknowledgments

Gunnar Myhre is gratefully acknowledged for providing the OsloCTM2 results. OsloCTM2 participates in the AeroCom phase 2 model intercomparison project (http://aerocom.met.no). Kirk Knobelspiesses participation in this research was supported by an appointment to the NASA Postdoctoral Program at the NASA Goddard Institute for Space Studies, administered by Oak Ridge Associated Universities through a contract with NASA. William Martin is supported by NASA Headquarters under the NASA Earth and Space Science Fellowship Program, Grant NNX-10AN85H. We acknowledge funding support from the NASA Glory Mission Project administered by Hal Maring and from the NASA ACE Formulation Study administered by David O'C. Starr.

#172897 - $15.00 USD Received 19 Jul 2012; revised 24 Aug 2012; accepted 25 Aug 2012; published 4 Sep 2012